Peer-reviewed version available at *Front. Genet.* **2020**, *11*; doi:10.3389/fgene.2020.00541

Article

MicroRNA-mRNA co-sequencing identifies transcriptional and post-transcriptional regulatory networks underlying muscle wasting in cancer cachexia

Geysson Javier Fernandez[1,2], Juarez Henrique Ferreira[1], Ivan José Vechetti-Júnior[1], Leonardo Nazario de Moraes[1], Sarah Santiloni Cury[1], Paula Paccielli Freire[1], Jayson Gutiérrez[3], Renato Ferretti[1], Maeli Dal-Pai-Silva[1], Silvia Regina Rogatto[4], Robson Francisco Carvalho[1]*.

[1] Department of Morphology, Institute of Biosciences, São Paulo State University (UNESP), Botucatu 18618-689, São Paulo, Brazil; fernandez.garcia@unesp.br (G.J.F); juarezhferreira@gmail.com (J.H.F); ijvechetti@gmail.com (I.J.V); leonardonmunesp@gmail.com (L.N.M); santiloni.cury@unesp.br (S.S.C.); paula.freire@unesp.br (P.P.F.); r.ferretti@unesp.br (R.F); maeli.dal-pai@unesp.br (M.D.-P.-S.)

[2] Grupo Inmunovirología, Facultad de Medicina, Universidad de Antioquia, UdeA, Medellín, Colombia

[3] Department of Plant Biotechnology and Bioinformatics, Ghent University, Ghent, Belgium; jayson.gutierrez@psb.vob-ugent.be (J.G)

[4] Clinical Genetics Department, University Hospital, Institute of Regional Health Research, University of Southern Denmark, Vejle, Denmark; Silvia.Regina.Rogatto@rsyd.dk (S.R.R)

* Correspondence: robson.carvalho@unesp.br; Tel.: +55-14-3880-0473

Abstract: Cachexia is a complex metabolic syndrome characterized by loss of skeletal muscle, leading to a significant weight loss that impacts patient morbidity and mortality. Given the complexity of gene regulatory networks that control gene expression, our objective was to perform an integrative mRNA and miRNA profiling to identify genetic programs that capture essential mechanistic details that promote muscle atrophy in cancer cachexia. Here, we used RNA sequencing to analyze miRNAs and mRNAs expression profiles in tibialis anterior (TA) muscles of the Lewis lung carcinoma model of cancer cachexia. In addition, we compared these findings with RNA-Seq data from C2C12 myotubes treated *in vitro* with the cachectic factors tumor necrosis factor-alpha (TNF-α) and interferon-gamma (IFN-γ). Extracellular matrix (ECM) alterations were validated by picrosirius staining, western blot, and fractal dimension analyses. We found 1,008 mRNAs and 18 miRNAs differentially expressed in cachectic mice. This set of genes was associated with the ECM, proteolysis, and inflammatory response. Enrichment analysis of transcriptional factor binding sites revealed activation of the atrophy-related transcriptional factors: NF-κB, Stat3, AP-1, and FoxO. Furthermore, the integration of mRNA and miRNA expression profiles identified post-transcriptional regulation by miRNAs of genes involved in ECM organization, cell migration, transcription factors binding, ion transport, and FoxO signaling pathway. C2C12 myotubes treated with TNF-α and IFN-γ similarly down-regulate subsets of ECM genes, including collagens. Our integrative analysis of miRNA-mRNA co-profiles comprehensive characterized regulatory relationships of molecular pathways and revealed miRNAs targeting ECM-associated genes in cancer cachexia. We also confirmed in C2C12 myotubes that changes in ECM-associated genes are dependent on inflammatory signaling of the cytokines TNF-α and IFN-γ.

Keywords: Lewis lung cancer, miRNAs, transcription factors, extracellular matrix, cancer cachexia

1. Introduction

Cancer cachexia is a multifactorial syndrome characterized by an ongoing loss of skeletal muscle mass that affects up to 80% of cancer patients, depending on the cancer type [1], and it represents the direct cause of at least 20% of cancer deaths [2]. The muscle wasting in cancer patients leads to a significant weight loss that affects the quality of life, response to radio- and chemotherapy, tolerance to treatment, and survival [3–7]. The loss of skeletal muscle mass - the most apparent symptom of cachexia - is mainly related to a metabolic dysregulation characterized by a resistance to anabolic signals, increased energy expenditure, and catabolism [8].

Several studies have linked cachexia to increased plasma levels of pro-inflammatory cytokines such as interleukin (IL)-1β, IL-6, tumor necrosis factor-alpha (TNF-α), and interferon-gamma (IFN-γ) [9]. These molecules alter the ubiquitin-proteasome, insulin-like growth factor 1 (IGF1)-Akt, and autophagy-lysosome pathways, which ultimately lead to an imbalance between muscle protein synthesis and degradation [9]. However, the molecular mechanisms by which these cytokines mediate muscle wasting are not entirely understood.

Recent advances in the mRNA transcriptome analysis have helped to unveil new molecular pathways, potential therapeutic targets, and biomarkers in cancer cachexia [10–18]. Genome-wide expression microarrays studies have also highlighted the importance of microRNAs (miRNAs) as an additional level of complex regulatory networks that post-transcriptionally control gene expression in muscle-wasting conditions [19–22]. While these studies have initially shown that global miRNA transcriptional profiles in wasting muscles seem to be peculiar to different catabolic conditions [21], it was subsequently demonstrated that the miRNA miR-29b contributes to multiple types of muscle atrophy, including those found in cardiac and cancer cachexia [23,24]. Skeletal muscle miRNA transcriptome profiling using RNA sequencing (RNA-Seq) is also highly informative in cancer cachexia and have identified novel miRNAs associated with the syndrome in patients with pancreatic and colorectal cancer [25]. This same study also reanalyzed two independent mRNA microarrays datasets and identified that the miRNA-targeted transcripts, in a tissue-specific context, are involved in myogenesis and inflammation pathways. In a mice model of cancer cachexia, miRNA sequencing combined with bioinformatics prediction analyses revealed that wasting muscles change the expression of miRNAs targeting transcripts that are essential for determining muscle size [26].

Although informative, these previous transcriptomic studies addressing muscle wasting in cancer cachexia did not explore different levels of gene expression regulation by integrating mRNA and miRNAs RNA-Seq data from the same set of muscle samples. Nevertheless, miRNA-mediated regulation of gene expression in cellular networks involves complex interplays among various miRNA targets through several mechanisms [27,28], which can be better addressed with simultaneous analysis of intrinsic interactions of biological entities across multiple omics layers. Thus, the identification of multi-omics features observed on the same set of samples provides a unique possibility for elucidating transcriptional and post-transcriptional regulatory networks during muscle wasting in cancer cachexia.

In the present study, we aimed to explore and integrate paired miRNA and mRNA co-profiles during skeletal muscle wasting in a mice model of cancer-induced cachexia. This comprehensive analysis allowed the identification of new miRNA targets and regulatory strategies controlling gene expression in skeletal muscle atrophy. Although the atrophic muscles of cachectic mice showed high heterogeneity in the transcriptional profile, we successfully identified a set of differentially expressed genes uniformly regulated across these cachectic samples. We also characterized regulatory relationships of molecular pathways, including miRNAs targeting extracellular matrix (ECM)-associated genes. Additionally, we used RNA-Seq to systematically examine mRNA levels in C2C12 cells treated *in vitro* with TNF-α and IFN-γ. This *in vitro* analysis confirmed congruencies between the *in vivo* gene expression results. Taken together, our results show that ECM-associated genes are dependent on inflammatory signaling and reveal miRNA-mRNA molecular networks that may play a role in the development of muscle wasting in cancer cachexia.

2. Results

2.1. Lewis lung carcinoma cells induced cachexia in mice.

As expected, all mice subcutaneously inoculated with Lewis Lung Carcinoma (LLC) cells developed cancer cachexia (LCC group) compared to mice injected with PBS (control group). The tumor was detected by palpation after seven days of cell injection in LLC; after 15 days, tumor site was visually detected as a skin projection; and after 22 days, when the animals were euthanized, tumor mass was observed under the skin. After euthanasia, the surgically exposed tumor was solid, vascularized, roughly spherical, measuring ~ 2 cm in diameter, and weighing ~ 4g (Supplemental Figs. S1A and S1B).

Although the LLC cell line is highly tumorigenic; metastases were not visually identified. Twenty-three percent of LLC mice died before the end of the experiment (Figure 1A). Consistently with cachexia syndrome, LLC group exhibited 14.4% of body weight (BW) loss after 22 days of LLC cell injection compared to the control group (Figure 1B). This BW reduction was associated with a loss of adipose tissue (Figure 1C) and skeletal muscle mass (Figure 1D). Cachexia was further confirmed by splenomegaly (Figure 1E and Supplemental Fig. S1C). Finally, among the studied muscles – tibialis anterior (TA), soleus (SOL), and gastrocnemius (GAS) – we selected TA for further analysis because its weight presented strong correlations between tumor weight (inverse correlation) and BW (positive correlation) (Figure 1F).

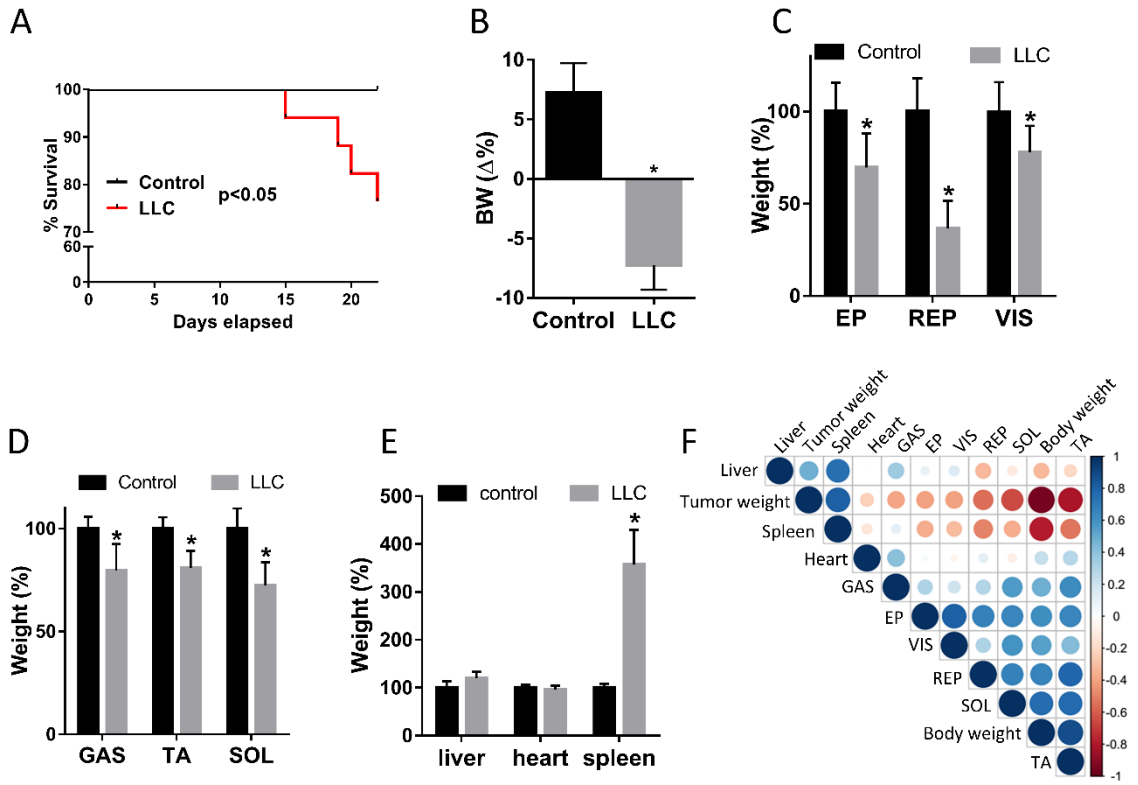

Figure 1. Lewis Lung Cancer (LLC) cells induce cachexia in mice. (A) Kaplan-Meier survival curves of control and tumor-bearing mice (LLC) groups. (B) Body weight (BW = %), defined as total BW - tumor weight, and reported as a percentage of the initial BW. (C) Epididymal (EP), retroperitoneal (RP), and visceral (VIS) fat weight loss in LLC respective to control. (D) Gastrocnemius (GAS), tibialis anterior (TA), and soleus (SOL) muscle weight loss in LLC respective to control. (E) Liver, heart, and spleen weight in LLC respective to control (F). Triangular Heatmap representing pairwise Pearson correlation of the different morpho-anatomical data; blue and red dots represents positive and negative correlation, respectively. Data are expressed as mean ± SD; control (n = 10) and LLC (n = 20). *p<0.05: statistical significance versus the control group (two-tailed t-test).

2.2. Comprehensive transcriptome characterization of muscle wasting revealed differential gene expression stability in cancer cachexia.

The transcriptome analysis of TA muscle revealed 11,436 genes (mapped reads > 32 by at least one of the sequenced samples) out of the nearly 45,000 mouse RefSeq genes. Principal Component Analysis (PCA) of 11,436 expressed genes was able to discriminate LLC and control samples (Figure 2A). A high heterogeneity on mRNA profiles of LLC group was evidenced by a spatial dispersion among these cachectic muscle samples. We found 1008 differentially expressed genes (DEG) ($p \leq 0.05$ and $|\text{fold change}| \geq 1.5$), of which 487 and 521 were up- and down-regulated, respectively. Unsupervised hierarchical clustering analysis of mRNAs expression data further confirmed the segregation between control and LLC groups and showed the DEG organized in four clusters (I-IV), according to their direction and variability of expression (Figure 2B): clusters I (n=386) and II (n=101) contain up-regulated genes, while clusters III (n=157) and IV (n=364) includes down-regulated genes. Considering the gene expression variability among LLC samples, clusters II and IV contain genes that are uniformly regulated (fold change % CV: 32.62 ± 15.50 and 32.49 ± 15.90, respectively; Figure 2C), whereas clusters I and III contain genes that demonstrated high variability in expression levels among LLC samples (fold change % CV: 65.60 ± 38.82 and 54.97 ± 15.42, respectively; Figure 2C).

Next, we explored the identity of the genes found within the clusters I-IV. Cluster I includes up-regulated genes that have a variable expression in LLC mice. The genes in cluster I encode proteins associated with the proteasome complex (e.g., *Trim63, Fbxo32, Ubc, Ubb, Psmd4, Psma7, Psmc2, Fbxo31,* and *Ube4a*), autophagosome (e.g. *Ctsl* and *Retreg1*), and the translation inhibitor Eif4ebp1 (Figure 2D and Supplemental Fig. S2A). Remarkably, cluster I includes the interleukin-6 receptor (*Il6ra*), which presented 5-logs range in expression variability (fold change varying from 1.5 up to 32) (Figure 2D). Cluster III contains down-regulated genes that have variable expression in LLC mice; this cluster includes genes associated with ECM (e.g., *Has3, Col15a1, Col22a1, Col9a1, Cpq,* and *Mmp15*) and muscle metabolism and contraction (e.g., *Myom3, Myh2, Myl3, Myoz2, Myh7, Lmod3, Synpo2,* and *Myl1*) (Figure 2D and Supplemental Fig. S2A). Cluster II comprises up-regulated genes that are uniformly regulated across LLC samples; these genes encode proteins related to immune cells system (e.g., *Selp, S100a9, Il1b, Cxcr2,* and *Csf3r*), ECM organization (e.g., *Mmp9, Mmp8,* and *TLL1*), and apoptotic process (e.g., *Cd300lf, Scarn1, Lcn2, Gadd45g,* and *Chac1*) (Figure 2D and Supplemental Fig. S2A). Cluster IV contains down-regulated genes that uniformly regulated in LLC samples; this cluster includes genes associated with ECM and sarcomere (Figure 2D and Supplemental Fig. S2A). Remarkably, both cluster III and IV contain genes related to the ECM (collagens) and sarcomere (myosins) but with differences in gene expression stability (low and high, respectively) within LLC samples.

Considering the variability in gene expression profiles across clusters I-IV, we determined a minimum number of differentially expressed genes able to differentiate cachectic and control groups, using genes that are uniformly regulated with high stability across cachectic samples. First, we used Pearson correlation values for each transcript to identify similarity across muscle samples (Supplemental Fig. S2B). This hierarchical grouping showed that the sample L1 had the most differential transcriptional profile in LLC group. Additionally, samples L2, L3, and L4 were clustered in a sub-group A, while samples L5 and L6 were clustered in a subgroup B (Supplemental Fig. S2B). Next, we determined the number of DEG between the subgroups A (n=3) or B (n=2) compared to the control group (n=4) (Supplemental Fig. S2C). Subgroup A has 56% less DEG (443, of which 145 are up- and 298 down-regulated), while subgroup B has more 57% DEG (1582, of which 630 are up- and 952 down-regulated) when compared to the number of DEG between LLC (n=6) and control groups (Supplemental Fig. S2C). Importantly, this 443 DEG identified in subgroup A was sufficient to effectively segregate both LLC and control groups (Supplemental Fig. S2D) and had a high intragroup stability (fold change % CV: 28.95 ± 10.02 and 27.30 ± 11.06, for up- and down-regulated genes, respectively) (Supplemental Fig. S2E and S2F). This set of DEG in subgroup A comprises genes associated with the ECM, proteolysis, and inflammatory response (Supplemental Fig. S2G).

Preprints (www.preprints.org) | NOT PEER-REVIEWED | Posted: 1 September 2019 doi:10.20944/preprints201909.0004.v1

Peer-reviewed version available at Front. Genet. 2020, 11; doi:10.3389/fgene.2020.00541

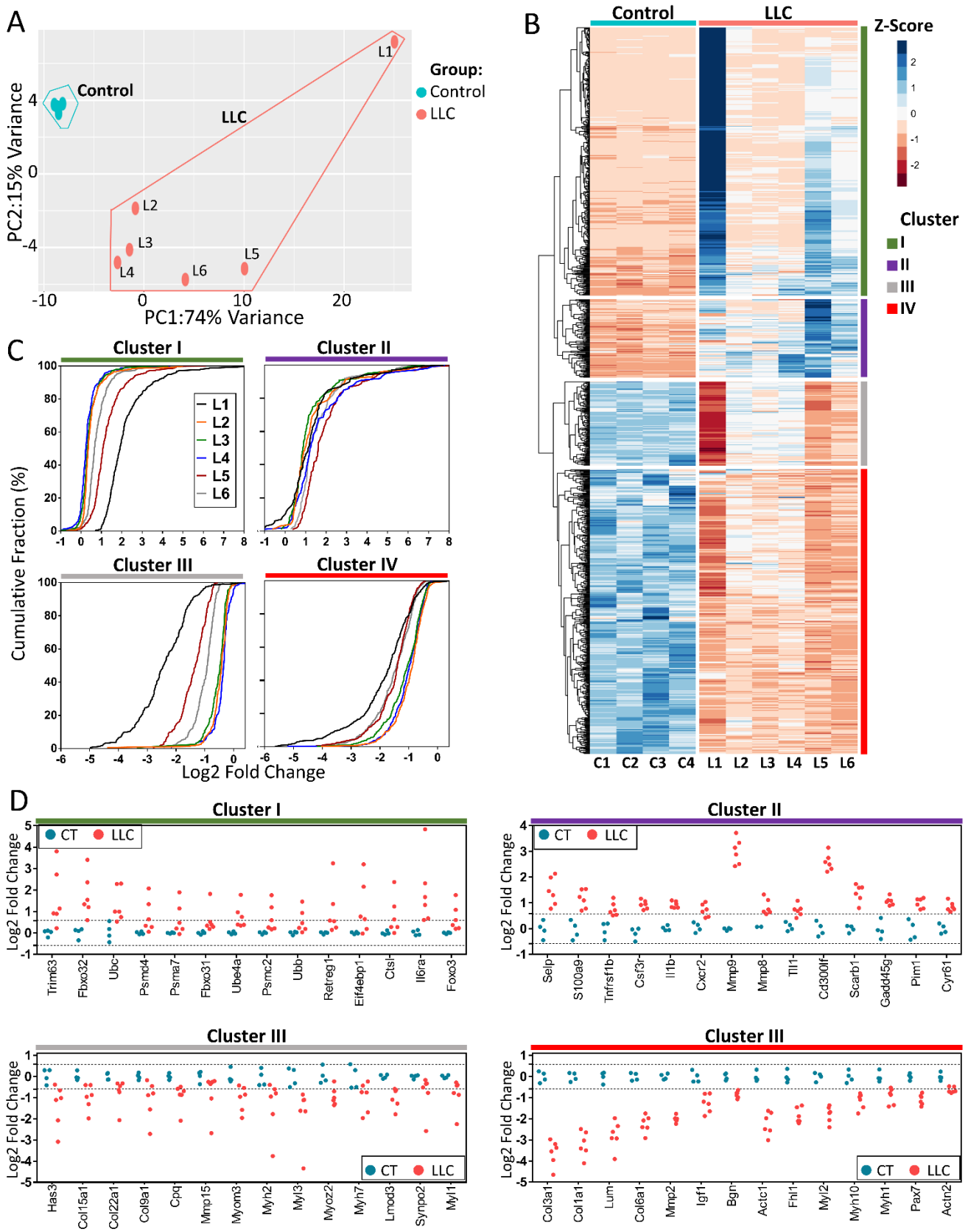

Figure 2. Comprehensive transcriptome characterization of muscles wasting revealed differential gene expression stability in cancer cachexia (A) Principal component analysis of the gene expression data of control and tumor-bearing mice (LLC) groups. The percentage of the variance of each principal component (PC1 and PC2) for control (C1-C4) and LLC samples (L1-L6). (B) Heatmap of 1008 Z-score normalized differentially expressed genes of control (C1-C4) and LLC samples (L1-L6) by unsupervised hierarchical clustering analysis

identified the clusters I (n=386), II (n=101), III (n=157), and IV (n=364). Down-regulated and up-regulated genes are shown in red and blue dots, respectively. (C) Cumulative frequency distribution of the differentially expressed genes (log2-fold change, x-axis) for LLC (L1-L6) vs. control samples, indicated as a percentage (%, y-axis) for each cluster (I to IV) identified in (B). (D) Dot plots of differentially expressed genes selected for each cluster (I to IV) identified in (B) to demonstrate the range in expression variability across genes. Light blue and pink dots represent control and LLC samples, respectively. The threshold for up- and down-regulated ($|\text{fold change}| \geq 1.5$) are indicated by dashed lines.

2.3. Relevant transcripts and regulatory pathways associated with muscle wasting in cancer cachexia.

We considered as biologically relevant transcripts for the muscle wasting those most abundant and with the highest degree of regulation. Initially, we used a scatter plot that integrated the degree of regulation (fold change; FC) and the abundance (Reads Per Kilobase Million; RPKM) of all transcripts (Figure 3A). Abundant transcripts presented subtle changes in gene expression when compared to rare transcripts. Notably, the up-regulated genes *Trim63*, *Fbxo32*, and *Ubc* - associated with proteasomal degradation pathway - presented the highest abundance and degree of change in expression (Figure 3A). Additionally, we identified the up-regulated transcripts *Ddit4* and *Eif4ebp1* (Figure 3A), which have been previously implicated in protein synthesis during skeletal muscle atrophy [29,30]. We also found upregulation in the expression of the antioxidant genes *Gpx3*, *Mt1*, and *Mt2* (Figure 3A), which have been described with a role in muscle repair in atrophic conditions [31–33].

We identified the down-regulation of the sarcomere genes *Myl1*, *Myh1*, *Fhl1*, *Gsn*, *Myl3*, and *Actc1* in cachectic muscle samples (Figure 3A). Interestingly, we found that the muscle-specific myoglobin (Mb) transcript is highly abundant and down-regulated (Figure 3A). In addition, a high degree of down-regulation of the ECM genes *Col3a1*, *Thbs4*, *Col6a1*, *Col1a1*, *Col1a2*, and *Col6a2* was identified. Finally, we detected low abundant transcripts with a high degree of regulation, including the *Il6ra* and the ECM remodeling genes *Mmp9* and *Mmp8* (Figure 3A).

The gene ontology analysis revealed 33 terms that were clustered in eight main modules that are relevant to muscle wasting, which include genes associated with the scaffold, cellular metabolism, cellular signaling, cellular differentiation, cellular immune system process, cellular respiration, proteolysis, and ion regulation (Figure 3B). Notably, some novelties were found such as the negative regulation of cell junctions (e.g. gap and tight junctions), carbohydrate metabolism (e.g. glycolytic process), cell differentiation (e.g. axonogenesis, angiogenesis, and PDGF signaling), and positive regulation of the immune cell system (e.g. neutrophil and leukocyte chemotaxis) (Figure 3B). Moreover, previously cachexia-associated terms such as negative regulation in the sarcomere, cell migration, and ECM genes, as well as positive regulation of genes involved in proteasome complex, autophagy, IL-6 signaling, and cell differentiation were detected (Figure 3B). We also identified the percentage of up- and down-regulated genes in each ontology term (Figure 3B). Consistent with the atrophic phenotype, this analysis demonstrated that all deregulated genes related to proteasome complex were up-regulated; while most of the deregulated genes related to myofibril and ECM were down-regulated (Figure 3B).

Considering the transcriptome variability across LLC samples, we also asked which pathways were enriched in LLC transcriptome when compared with the reduced set of genes enriched explicitly in the LLC subgroup A. This analysis confirmed changes in the expression of genes associated with protein degradation such as proteasome complex, the autophagosome, and macroautophagy (Figure 3B).

Preprints (www.preprints.org) | NOT PEER-REVIEWED | Posted: 1 September 2019 doi:10.20944/preprints201909.0004.v1

Peer-reviewed version available at Front. Genet. 2020, 11; doi:10.3389/fgene.2020.00541

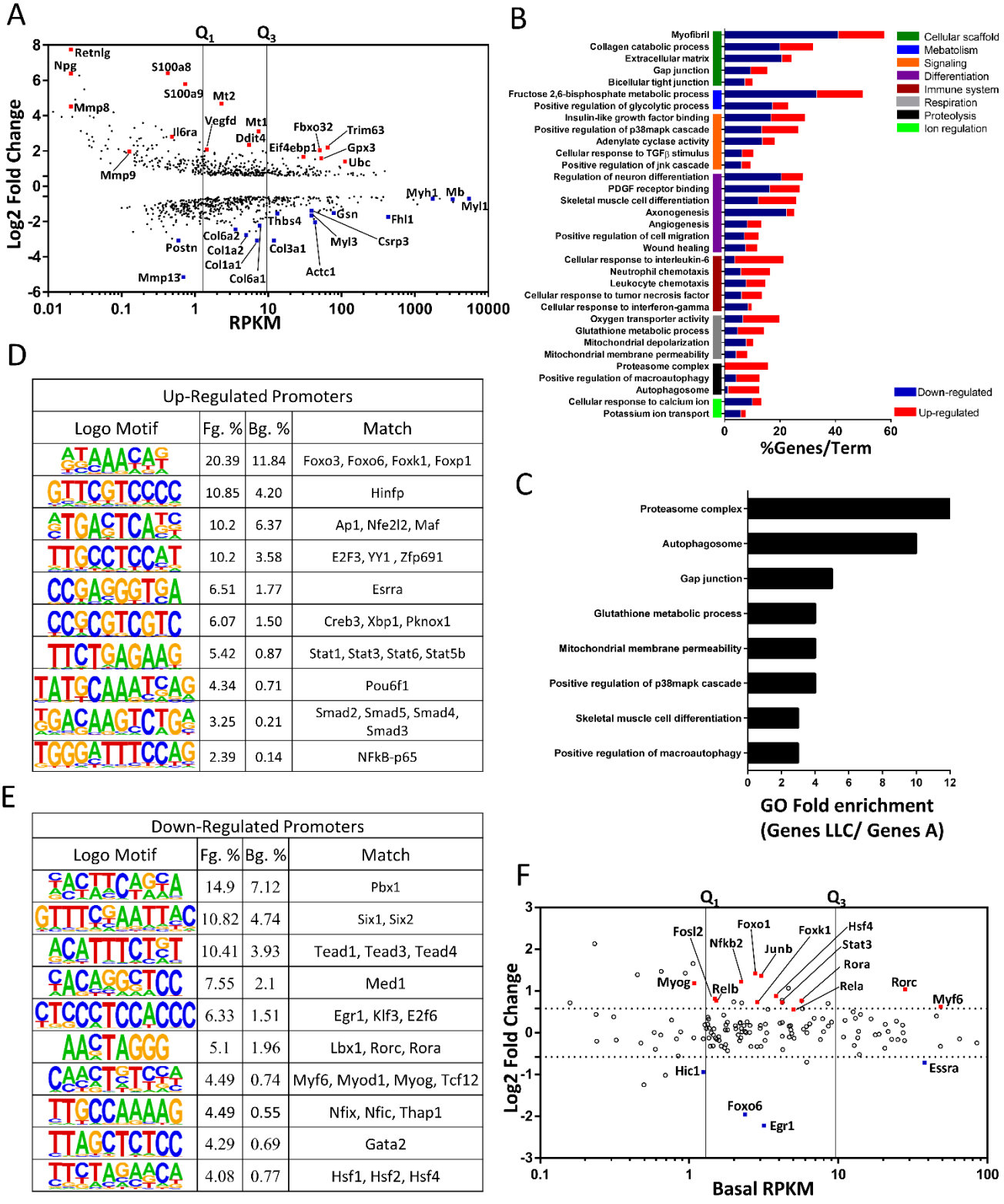

Up-Regulated Promoters

Logo Motif	Fg. %	Bg. %	Match
	20.39	11.84	Foxo3, Foxo6, Foxk1, Foxp1
	10.85	4.20	Hinfp
	10.2	6.37	Ap1, Nfe2l2, Maf
	10.2	3.58	E2F3, YY1 , Zfp691
	6.51	1.77	Esrra
	6.07	1.50	Creb3, Xbp1, Pknox1
	5.42	0.87	Stat1, Stat3, Stat6, Stat5b
	4.34	0.71	Pou6f1
	3.25	0.21	Smad2, Smad5, Smad4, Smad3
	2.39	0.14	NFkB-p65

Down-Regulated Promoters

Logo Motif	Fg. %	Bg. %	Match
	14.9	7.12	Pbx1
	10.82	4.74	Six1, Six2
	10.41	3.93	Tead1, Tead3, Tead4
	7.55	2.1	Med1
	6.33	1.51	Egr1, Klf3, E2f6
	5.1	1.96	Lbx1, Rorc, Rora
	4.49	0.74	Myf6, Myod1, Myog, Tcf12
	4.49	0.55	Nfix, Nfic, Thap1
	4.29	0.69	Gata2
	4.08	0.77	Hsf1, Hsf2, Hsf4

Figure 3. Relevant transcripts and regulatory pathways associated with muscle wasting in cancer cachexia. (A) Scatterplot comparing abundance (RPKMs, x-axis) and their degree of expression (log2 fold change, y-axis). Each dot represents differentially expressed genes (DEG; fold-change > 1.5 and FDR < 0.05; Wald test) potentially relevant to muscle wasting (red and blue dots represents up- and down-regulated transcripts, respectively). Vertical lines represent thresholds for low, medium and high abundance genes as defined by quartiles (Q1 and Q3) (B) Gene-term enrichment analysis of DEG in tibialis anterior of Lewis Lung Cancer (LLC) tumor-bearing mice showing the top canonical pathways. The colored horizontal bars represent the percentage of genes presented in the data set compared to the total number of genes in each term (% Genes/Term). The fraction of

up- and down-regulated genes (horizontal bars) in each term are shown in red and blue, respectively. The vertical colored bars (y-axis) represent major gene terms modules. (C) Gene-Ontology analysis of DEG from LLC vs. LLC subgroup A samples. Each horizontal black bar represents the ontology term fold enrichment compared to the total number of genes in each term. De novo motif analysis performed on promoters (-300 and +50 relative to Transcription Start Site, TSS) of up- (D) and down-regulated (E) genes. Motifs were compared by using the transcription factor JASPAR database to determine the closest annotated matches. Percentage (%) represents a fraction of foreground (Fg) and background (Bg) sequences that contain at least the occurrence of one motif. (F) Scatterplot comparing abundance (Basal RPKMs, x-axis) and their degree of expression (log2 fold change, y-axis). Each dot represents a differentially expressed gene (DEG; fold-change > 1.5 and FDR < 0.05; Wald test) encoding for transcription factors (red and blue dots, up- and down-regulated transcripts, respectively). Vertical lines represent thresholds for low, medium, and high abundance genes as defined by quartiles (Q1 and Q3).

2.4. Transcriptional factors motifs enriched during muscle wasting in cancer cachexia

The transcriptional profile can provide a step towards the identification of key transcription factors that regulate gene expression. In the present study, this was achieved by enrichment analysis of transcriptional motifs in the promoter sequences of the differentially expressed genes (Figure 3D and 3E). The promoters of the up-regulated genes revealed a motif enrichment for the Forkhead transcription factor (FoxO) (Figure 3D). However, when we analyzed the changes in expression and abundance of FoxO family members genes, only *FoxO1* and *FoxO6* were up- and down-regulated, respectively (Figure 3F). The promoters of the up-regulated genes also revealed binding sites for transcriptional factors within the NF-κB and STAT families (Figure 3D). These results were supported by our gene set enrichment analyses (Figure 3B). Additionally, components of the NF-κB and STAT families were up-regulated: *Rela, RelB, Nfkb2* (*NF-κB*), and *Stat3* (*STAT*) (Figure 3F). We found enrichment of the AP-1 transcription factor, as well as the up-regulation of *Junb* and *Fosl2*, which are translated into proteins that constitute the AP-1 heterodimer (Figure 3F). We also found enrichment of other transcriptional factors without a change in their expression (Figures 3D and 3F); among these are transcription factors related to cell cycle regulation (*E2f3, Yy1,* and *Creb3*), unfolding protein response (*Xbp1*), and the SMAD family (*Smad2, Smad3, Smad4* and *Smad5*).

Interestingly, promoters of down-regulated genes also revealed motif enrichment of transcriptional factors related to myogenesis (Myf6, Myod1, Myog, Tcf12, Pbx1, lbx1, Nfix, and Nfic), lipid homeostasis (Rora and Rorc), energy metabolism (Med1), and muscle fiber-type specification (Six1, Six2, Tead1, Tead3, Tead4, Egr1, Klf3, Hsf1, Hsf2, and Hsf4) (Figure 3E). However, only genes coding for the transcription factors *Myf6, Myog, Rorc, Rora,* and *Egr1* changed their expression (Figure 3F).

2.5. miRNAs associated with muscle wasting in cancer cachexia

Our experimental strategy was to simultaneously evaluate miRNAs expression via high-throughput sequencing in the same set of samples used for transcriptomic analyses (sample L4 failed sequencing quality control and were excluded from further analysis). Out of 1915 mature miRNAs, 302 were expressed in skeletal muscle (mapped reads > 32 in at least one of the sequenced samples). Eighteen miRNAs were differentially expressed (FDR ≤ 0.05 and |fold change| ≥ 1.5) in muscle wasting during cancer cachexia in comparison to controls (13 up and five down-regulated, Figure 4A).

PCA and clustering analysis showed that these 18 miRNAs did not cluster samples accordingly to their experimental groups, as we found for mRNAs (Figures 2A and 2B). Furthermore, 44% of differentially expressed miRNAs in LLC muscle samples were expressed at low levels and degree of regulation (Figure 4C). Notably, miR-10b-5p was regulated at high levels in atrophying muscles (Figure 4C). The differentially expressed miRNAs also included the miR-29b-3p, miR-146a-5p, miR-146b-5p, and miR-181c-3p, which have been previously studied in a skeletal muscle context [24,34,35].

Preprints (www.preprints.org) | NOT PEER-REVIEWED | Posted: 1 September 2019 doi:10.20944/preprints201909.0004.v1

Peer-reviewed version available at Front. Genet. 2020, 11; doi:10.3389/fgene.2020.00541

Interestingly, the MyomiRs mir-208a, mir-208b, mir-499, miR-133a, miR-133b, and miR-1 were not differentially expressed in the LLC group.

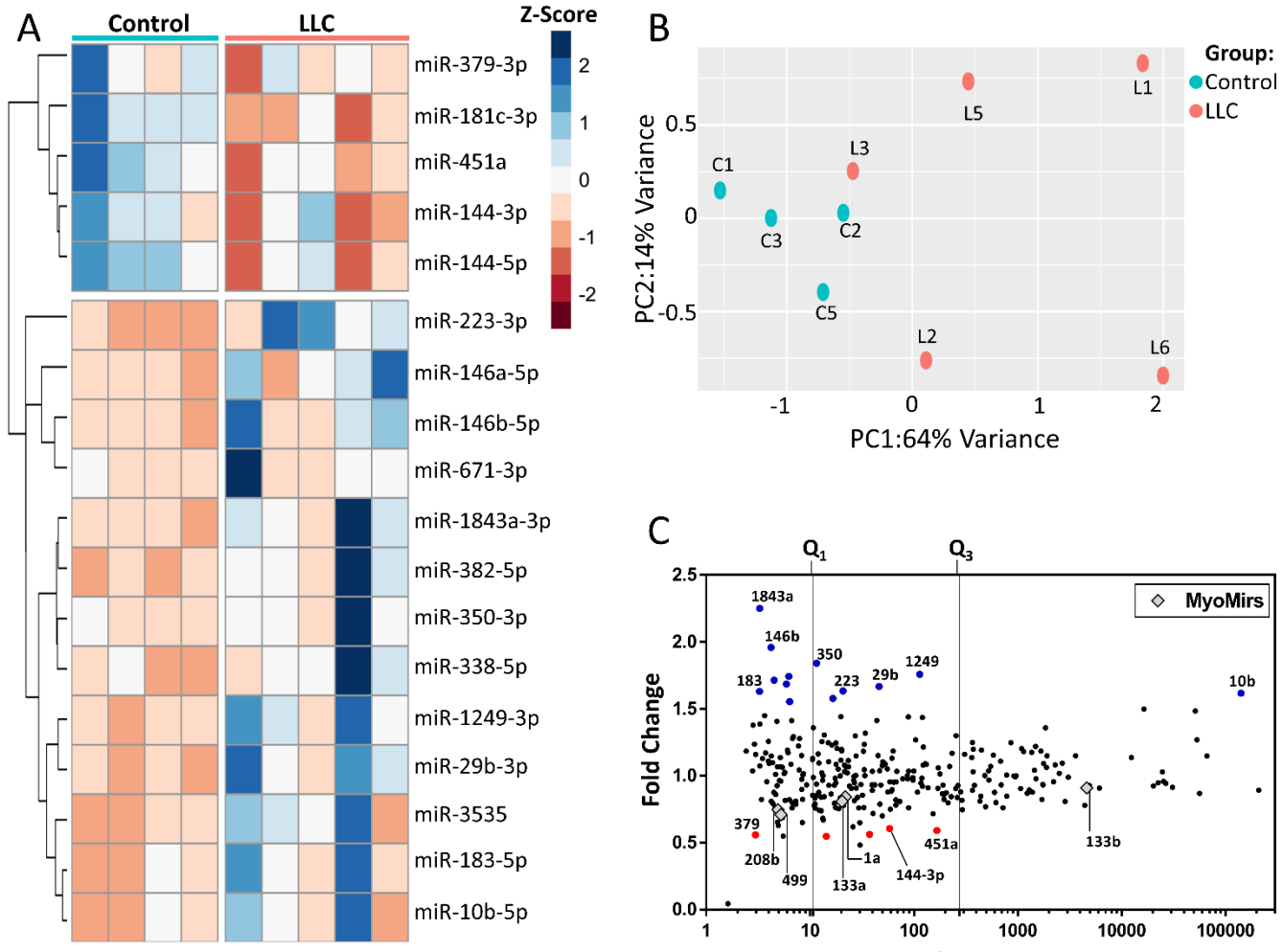

Figure 4. Differentially expressed miRNAs in cancer cachexia. (A) Principal component analysis of the gene expression data of control and tumor-bearing (LLC) mice. The percentage of the variance of each principal component (PC1 and PC2) for control (C1-C4) and LLC (L1-L3, L5-L6) samples. The sample L4 did not pass the quality filters, and it was removed from the analysis (B) Heatmap of 18 Z-score normalized differentially expressed miRNAs of control (C1-C4) and LLC (L1-L3, L5-L6) samples by unsupervised hierarchical clustering analysis. Down-regulated and up-regulated miRNAs with absolute values of fold-change > 1.5 and FDR < 0.05 (Wald statistics) are shown in red and blue, respectively. (C) Scatterplot comparing abundance (Counts per Million, CPM; x-axis) and their degree of expression (log2 fold change, y-axis). Each dot represents differentially expressed miRNAs (fold-change > 1.5 and FDR < 0.05; Wald test), and red and blue dots (up- and down-regulated miRNAs, respectively) highlight potentially relevant miRNAs associated with muscle wasting. Gray diamonds represent the muscle-specific miRNAs (MyomiRs). Vertical lines represent thresholds for genes with low, medium, and high abundance, as defined by quartiles (Q1 and Q3).

2.6. miRNAs associated with muscle wasting in cancer cachexia

To improve the accuracy of our *in-silico* mRNA target prediction used to identify potential mRNA targets of the differentially expressed miRNAs, we applied a parallel miRNA-mRNA expression profile, as previously described [36]. This approach considers opposite directions of deregulated expression between miRNA and target mRNAs in the same set of samples. We found a network with 171 interactions between 18 miRNAs and 131 target genes (Figure 5A). This analysis revealed that the upregulated miRNA miR-350-3p has a higher number of target transcripts (n=47). Interestingly, miR-29b-3p presented 22 potential targets, including many transcripts that encode

proteins related to the ECM. Additionally, we found that repressed miRNAs do not share target transcripts. Furthermore, some transcripts such as Map2k6, Ptpn3, Mettl21c, Plxdc2, Ppargc1b, Rgs5, and Vegfa were found to be co-regulated by up to three upregulated miRNAs (Supplemental Table S1).

Based on the integrative miRNA-mRNA analysis, we identified enriched pathways for deregulated genes targeted by differentially expressed miRNAs (Figure 5B). Gene-Ontology analysis revealed miRNA interactions affecting genes regulating mainly the ECM, but also cell migration, transcription factor binding, ion transport, and FoxO signaling. To elucidate the functions of these complex interactions between mRNAs and miRNAs in cancer cachexia, we constructed a regulatory network displaying predicted and validated interactions between the miRNAs and target mRNAs, considering physical and pathway protein-protein interactions (Figure 5C-D). We found sub-networks such as those related to ECM organization (Figure 5C), cell migration (Figure 5D), and transcription factors (Figure 5E). ECM organization network (Figure 5C) contains a set of nine collagen transcripts, including validated targets of the miR-29b-3p. Furthermore, we found predicted interactions for miR-1843a-3p, miR-350-3p, miR-223-p, and miR-3535 with ECM components such as *Col6a1, Timp2, Mmp15, Dcn,* and *Actn2*. These identified networks share the miRNAs mir-29b-3p, mir350-3p, and miR-3535, suggesting a pleiotropic effect of these miRNAs on the ECM of atrophying muscles in cancer cachexia.

Preprints (www.preprints.org) | NOT PEER-REVIEWED | Posted: 1 September 2019 doi:10.20944/preprints201909.0004.v1

Peer-reviewed version available at Front. Genet. 2020, 11; doi:10.3389/fgene.2020.00541

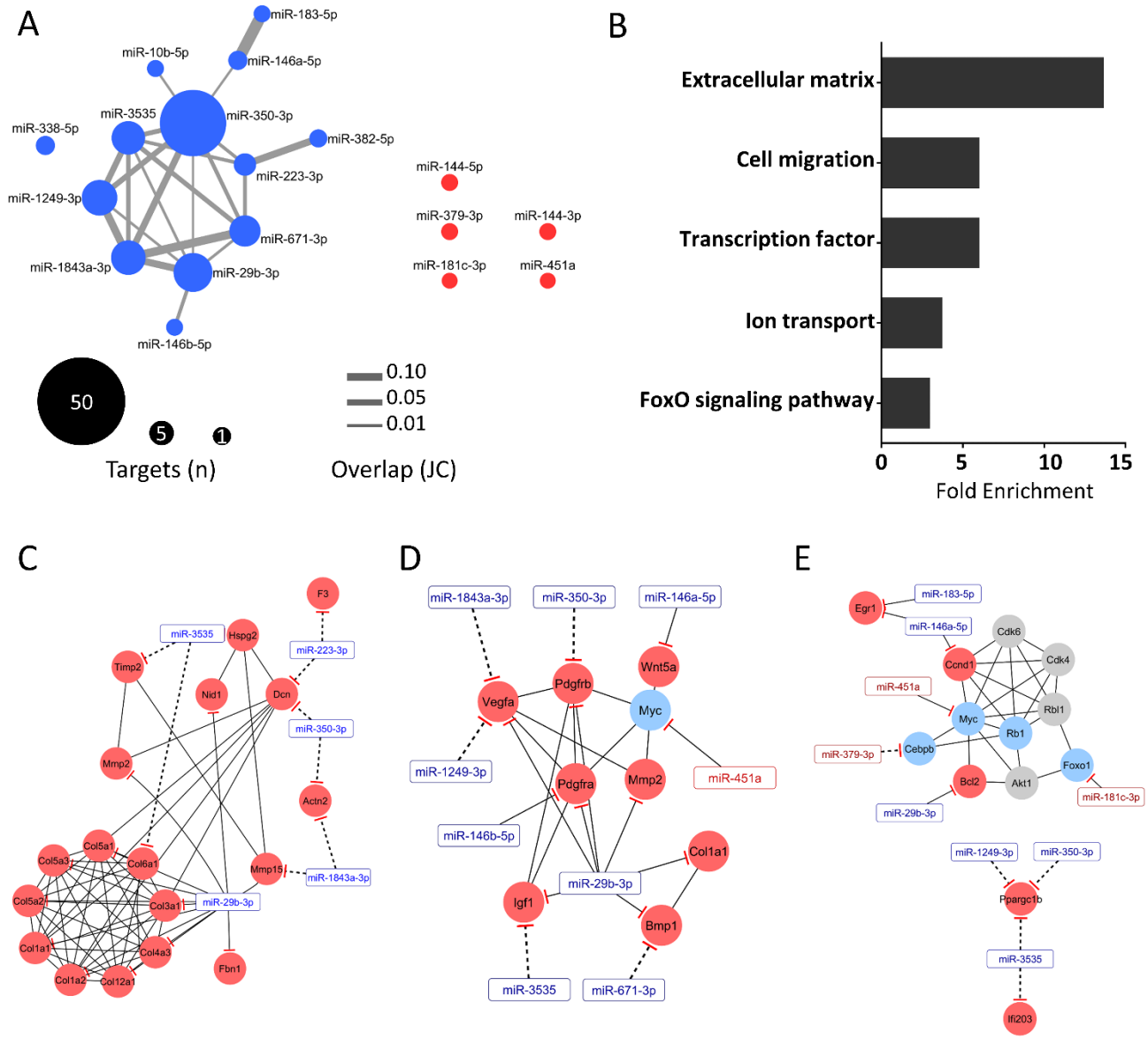

Figure 5. Integrative analysis revealed a set of extracellular matrix mRNAs regulated by miRNAs. (A) The network generated is consisted of 171 interactions between 18 miRNAs and 131 target transcripts. Up- and down-regulated miRNAs (fold-change > 1.5 and FDR < 0.05; Wald test) are represented by blue and red nodes, respectively. Node size indicates the number of miRNA-target transcripts, and gray edge width denotes overlapping miRNA-target transcripts measured by the Jaccard coefficient (JC). (B) Gene-Ontology analysis of the mRNAs predicted and validated as regulated by microRNAs. Each horizontal black bar represents the ontology term fold enrichment compared to the total number of genes in each term. Regulatory network displaying predicted (dashed lines) and validated (solid lines) interactions between the miRNAs (rectangle) and target mRNAs (circles), and physical and pathway protein-protein interactions (solid lines) for extracellular matrix (C), cell migration (D), and transcription factors (E). Up- and down-regulated miRNAs (fold-change > 1.5 and FDR < 0.05; Wald test) are represented by blue and red nodes, respectively. Grey nodes represent non-regulated genes.

2.7. TNF-α/IFN-γ signaling in C2C12 myotubes also down-regulates ECM genes found in cancer cachexia.

We next treated C2C12 myotubes with TNF-α/INF-γ. These cytokines act synergistically to trigger skeletal muscle cells atrophy both *in vitro* and *in vivo* models [37,38], and thus the identification of shared deregulated genes in both models may identify genes affected by chronic inflammation. The synergistic TNF-α/INF-γ signaling reduced myotube diameter in ~ 30% compared

to the untreated cells (Figure 6A), and deregulated 1794 genes. We found an overlap of 587 genes between our *in vitro* an *in vivo* models (67% of the DEG, Figure 6B). Moreover, 201 and 221 genes (up- and down-regulated, respectively) share the same direction of expression change in both conditions (Figure 6B). Gene ontology analysis identified that commonly up-regulated genes are enriched for NF-kB pathway (Figure 6C), while the down-regulated genes are enriched for ECM (Figure 6D).

Together, our results point out to a crucial role of ECM remodeling in skeletal muscle atrophy in cancer cachexia. TA muscle cross-sectional area stained with Picrosirius red in LLC tumor-bearing mice presented reduced total collagen deposition (Figure 7A and 7B) and ECM disarrangement (Figure 7C), as revealed by picrosirius red staining area and fractal dimension analysis, respectively. The reduction of ECM was further confirmed by the reduced protein levels of collagen alpha-1 type I collagen (COL1A1), one of the main structural components of the ECM in skeletal muscle tissues (Figure 7D).

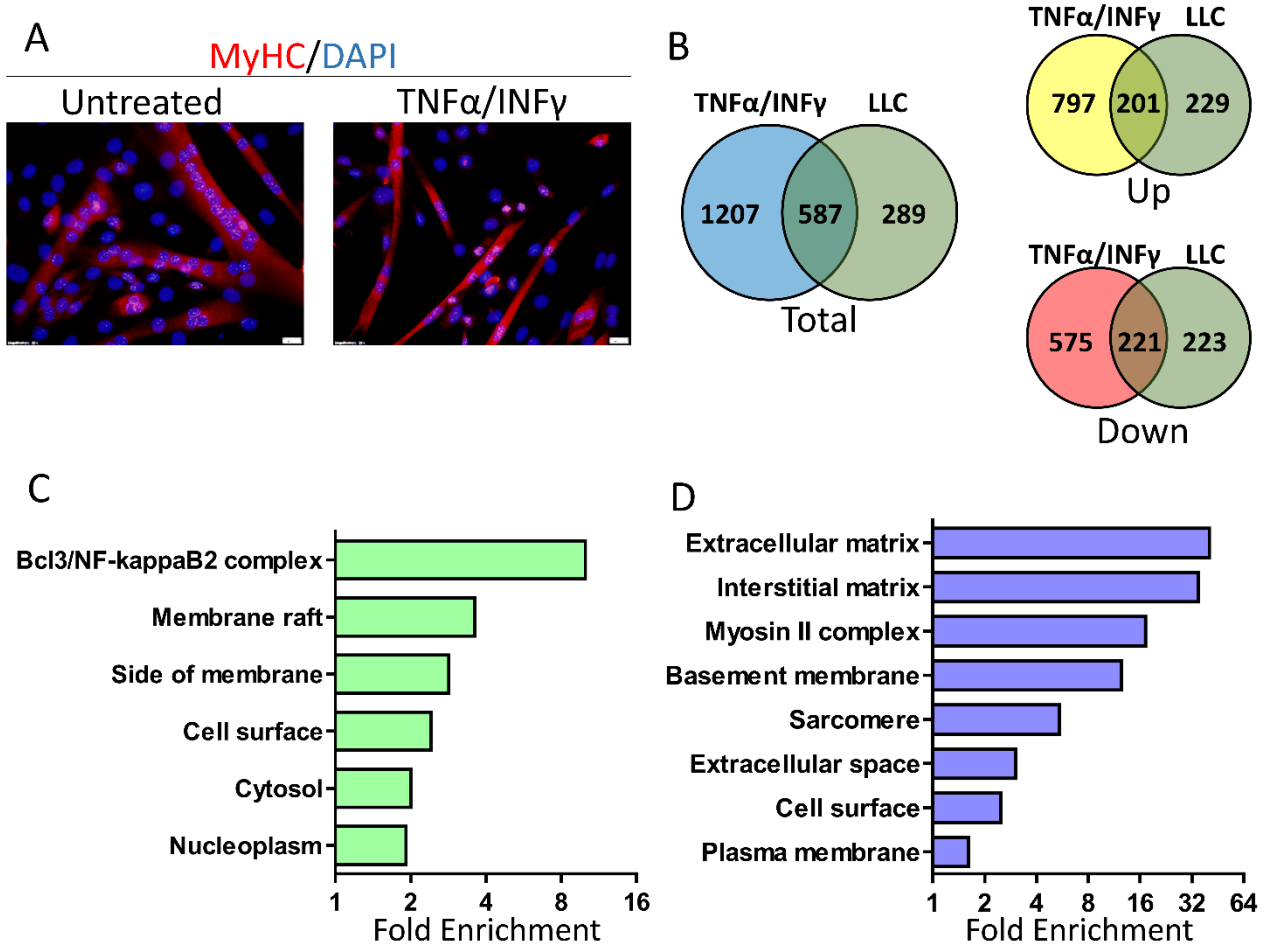

Figure 6. TNF-α/IFN-γ signaling in C2C12 myotubes also downregulate ECM genes found in cancer cachexia. (A) Immunofluorescence staining of C2C12 myotubes treated with TNF-α/INF-γ for 20h or control (untreated). Myosin Heavy Chain (MyHC). Scale bars: 20 μm. (B) Venn diagrams showing shared differentially expressed genes (total, up- and down-regulated) in Lewis Lung Cancer (LLC) tumor-bearing mice and TNF-α /INF-γ-C2C12 treated myotubes, compared to their respective control groups. Gene-ontology analysis of shared up- and down-regulated (C and D, respectively) between Lewis Lung Cancer (LLC) tumor-bearing mice and TNF-α /INF-γ-C2C12 treated myotubes; horizontal bars represent the ontology term fold enrichment presented in the data set compared to the total number of genes in each term.

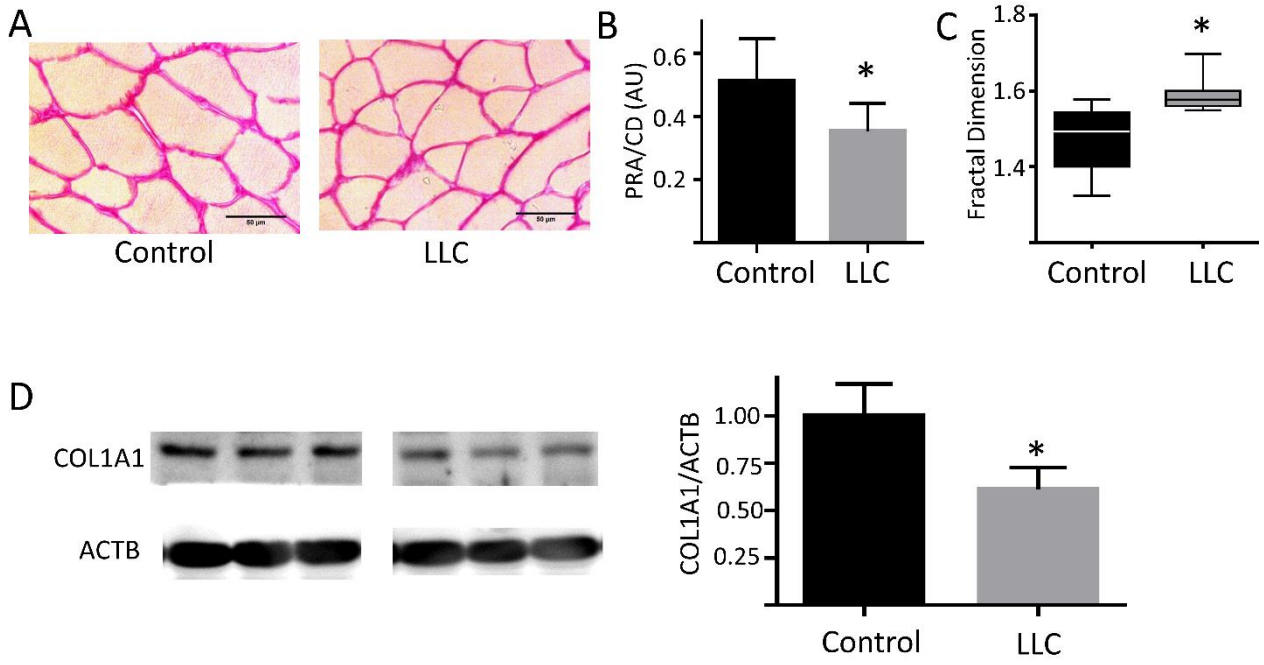

Figure 7. Extracellular matrix remodeling in skeletal muscle during cancer cachexia. (A) Histological sections of tibialis anterior (TA) muscle stained with Picrosirius-red staining at 20x magnification of control and LLC tumor-bearing mice muscle (B) Quantitative analysis of Picrosirius-red staining areas (PRA) normalized by cell density (CD) (C) Fractal dimension analysis of TA Picrosirius-red staining areas of control and LLC tumor-bearing mice muscle (D) Proteins levels of Col1a1 in TA muscle of control and LLC tumor-bearing mice; blots were normalized by α–actin protein levels

3. Discussion

Despite advances in the study of cancer cachexia, its pathogenesis is complex and remains incompletely understood [39]. Thus, it is necessary to identify signaling pathways as well as transcriptional and post-transcriptional events underlying skeletal muscle atrophy in this condition. We used paired microRNA-mRNA co-profiles in wasting muscles of cachectic mice, which unveiled ECM remodeling events potentially regulated by miRNAs. Although our transcriptomic analysis demonstrated a high heterogeneity on mRNA profiles of cachectic mice, we successfully identified a minimum number of differentially expressed genes that were uniformly regulated with low variability across cachectic samples. We further identified that ECM remodeling is dependent on inflammatory signaling of cytokines such as TNF-α and IFN-γ. Thus, in addition to the well-known down-regulation of sarcomere proteins genes, other transcripts encoding ECM structural proteins potentially regulated by miRNAs may contribute to the development of skeletal muscle wasting in cancer cachexia.

Our RNAseq data significantly expands previous genome-wide studies in cancer cachexia by integrating mRNA and microRNA transcriptome profiling from the same set of muscle samples. This strategy allowed us to identify miRNA targets with higher accuracy. Moreover, we used a high number of biological replicates (6 cachectic and four controls), which added higher precision and sensitivity for the identification of transcriptional and post-transcriptional events. Our transcriptomic data reliably differentiated muscle samples from cachectic and control mice. Notably, an inter-individual variation in the mRNA expression was evidenced in cachectic mice, which may be linked to individual genetic factors and stochastic tumor growth events that may determine the development and progression of muscle wasting. In fact, studies in rodent models show heterogeneity in the occurrence of cachexia [40,41]. This characteristic is also found in human neoplasms, which shows variability in the prevalence and severity of cachexia among patients with the same diagnosis and cancer stage [39,42]. Importantly, we found genes commonly associated with cachexia that demonstrated high variability in expression levels among cachectic mice, which may help to explain the variability in the prevalence and severity of the syndrome. For example, the high

variable up-regulated genes are related to protein catabolism (e.g., *Trim63* and *Fbxo32*, Figure 2), while the high variable down-regulated genes are mainly associated with sarcomere and ECM. This variability in the expression profile of these set of genes may help to explain why protein catabolism genes in human studies have failed to recapitulate the findings from murine models [14,43]. This variability in gene expression, also known as noise, has been described as an essential feature of any biological system [44], and previous gene expression studies have been able to classify different states of diseases based on this variability [45–48].

To generate a complete picture of transcriptome content and dynamics, we explored the differential expression data to identify transcriptional factor-binding motifs. Our motif analysis for up-regulated genes identified enrichment for several transcription factors, including FoxO, NF-κB, AP-1, Stat3, and Smad. These factors have already been described in the regulation of muscle atrophy by activating genes related to the proteolytic ubiquitin-proteasome, autophagy-lysosomal, metabolic adaptation, myogenesis, differentiation, and immune-modulation [49–54]. Similarly, the motif analysis also showed that down-regulated genes were associated with myogenic transcription factors [55–57], metabolism [58], fiber transition [59,60], muscle contraction [61]. Most importantly, our motif analysis revealed transcription factors that have not yet been reported or identified previously in cancer cachexia. These factors are related to cell cycle and myogenesis (E2f3, Yy1, and Creb3) [62–64], unfolding protein response (Xbp1) [65], and muscle fiber metabolism (ESRRA) [66]. Also, we identified an increased expression of the myogenic regulatory factors *Myf6* and *Myog*. Interestingly, it has been demonstrated that over-expression of Myf6 inhibits the transcription of sarcomeric proteins by inhibiting Mef2 [67]. On the other hand, Myog induces the expression of the atrogenes *Trim63* and *Fbxo32* [68]. Together, the differential expression profile of transcriptional factors suggests that muscle atrophy in cancer cachexia can only be understood in the context of simultaneous signaling pathways activated by different transcriptions factors. This is in contrast with a previous report indicating Foxo as a single master regulator controlling muscle wasting during cancer cachexia [18]. The combinatory action of transcriptional factors is supported by the long-standing view that specific combinations of transcriptional factors act cooperatively or in sequential steps in the regulation of gene expression [69]. Also, it has been recently demonstrated that the combination of the transcriptional factors NF-κB, SRF, and IRF control gene expression through logical OR gates in macrophages [70]. Moreover, the cooperative interaction of the transcriptional factors STAT3 and NF-κB promotes muscle atrophy [38], further demonstrating cooperative actions of transcription factors controlling gene expression in muscle-wasting conditions.

Even though transcriptional factors are essential to understand gene regulation, it is also crucial to identify post-transcriptional regulations mediated by miRNAs, which induce mRNA decay and inhibit translation [71]. To better understand the miRNA-mRNA interactome in cancer cachexia, we combine the miRNA-mRNAs expression co-profiles in the same set of muscle samples. This analysis allowed us to identify biological processes such as ECM, cell migration, and transcription as regulated by miRNAs during muscle wasting in cancer cachexia. Within these interactions, we highlight the up-regulation of the miR-29b-3p, which regulates a plethora of processes such as migration, ECM, and myogenesis. The miRNA miR-29b-3p has been described as a critical regulator in a variety of processes such as myogenesis [72] and muscle atrophy [24,36], and it has a multiplicity of targets in skeletal muscle cells, including collagens transcripts [73], *YY1* [74], *p85* [75], and *IGF-1* [76].

It is worth noting that the same cancer cachexia mice model as ours has been previously used to identify the global miRNA expression profile in wasting muscles [26], but only miR-223-3p was shared as deregulated with our data. Additionally, our set of deregulated miRNAs does not overlap with the muscle miRNA expression profile from other mice model of cancer cachexia or cachectic patients [25,77]. This may be a consequence of the highly dynamic post-transcriptional regulation mechanisms exerted by miRNAs, which may act buffering fluctuations in gene expression and conferring robustness in signaling outcomes for specific regulatory networks [78]. Another plausible explanation is that different miRNAs sharing the same seed regions target the same transcripts or pathways during the development of muscle wasting [78]. Consequently, target contextual features

determine miRNA target recognition and regulatory outcome as well as RNA interaction networks in specific biological contexts [79], reinforcing the importance of the use of parallel expression profile of mRNA and miRNA, as used herein, to gain further insights into post-transcriptional controls underlying muscle wasting in cancer cachexia.

Collectively, our integrated mRNA and miRNA data pointed out to the remodeling of the ECM components in the wasting muscles. These results are in agreement with previous studies showing the down-regulation of ECM genes in cancer and cardiac cachexia [18,36,80]. Accordingly, it has been previously demonstrated that the reduction of collagen gene expression is highly regulated by different cytokines, including TNF-α [81,82]. The effects of TNF-α stimulation are mediated by NF-κB, which binds to the promoter region of collagen genes and negatively control their expression [83]. On the other hand, IFN-γ increases the expression of CIITA, which forms a co-repressor complex that represses the transcription of collagen genes [84]. Our transcriptome data from C2C12 muscle cells treated with TNF-α/IFN-γ further support this fact by presenting not only a reduction in the expression of collagen genes but also in other genes involved in ECM assembly, including Ogn. Our group had previously shown that Ogn affects the proliferation and differentiation of C2C12 muscle cells [85]. A previous study has also investigated the potential contributory factors outside the fiber within the muscle microenvironment in humans and animals and found that Pax7 responds to NF-κB by impairing the regenerative capacity of myogenic cells to drive muscle wasting in cancer cachexia [80]. Thus, our findings suggest that in addition to alterations in the regenerative capacity of myogenic cells, miRNA-mediated regulation of the ECM also contribute to muscle wasting in the syndrome.

While our study identified transcriptional and post-transcriptional regulatory networks underlying muscle wasting in cancer cachexia, our *in-silico* approach is limited in several respects. Firstly, although our work describes the variability in the expression of specific sets of genes, further studies are needed to establish how inter-individual variation in gene expression affects the prevalence and severity of the syndrome. Secondly, our study reveals several transcription factors potentially involved in the regulation of cachexia genetic program, and experiments are still necessary to quantify their sequence-specific DNA-binding activity. In the same way, we predicted miRNA-target interactions that deserve experimental verification.

4. Materials and Methods

4.1. Lewis lung carcinoma (LLC) model of cancer cachexia

To generate the LLC model of cancer cachexia, we used 8-week old, healthy C57BL/10 male mice obtained from a breeding colony, maintained by our institutional animal care facility at the Sao Paulo State University (UNESP, Botucatu, Sao Paulo, Brazil). The animals were housed in cages under a 12-h light/dark cycle with food and water ad libitum. Before inoculation into mice, LLC cells (ATCC® CRL-1642™) were cultured in Dulbecco's modified Eagle's medium (DMEM, Thermo Fisher Scientific, USA) supplied with 10% of fetal bovine serum (FBS, Thermo Fisher Scientific, USA) and 1% penicillin/streptomycin (Thermo Fisher Scientific, USA) and maintained in a 5% CO2, 37°C humidified incubator. After three days of acclimation to their environment, mice were randomly assigned into two groups. Twenty mice (LLC group) were inoculated subcutaneously with a total of 1.5 x10^6 LLC cells (7.5 x 10^5 cells in 0.1 mL PBS, in each flank). Ten mice (control group) were injected with equal volumes of 1X PBS.

LCC and control mice were weighed daily and studied after 22 days after LLC cells inoculation when the LLC group had developed overt cachexia. The animals were euthanized upon anesthesia with intraperitoneal ketamine and xylazine (100 mg/kg and 10 mg/kg, respectively). The tumor diameter and body weight were measured; and the TA, SOL, and GAS muscles were collected, weighed, and then snapped frozen in liquid nitrogen for further analyses. These muscles were chosen based on their fiber composition: TA muscle has a higher proportion of glycolytic fast-twitch fibers;

SOL muscle has a higher proportion of oxidative slow-twitch fibers; and the GAS muscle, which comprises both fiber types.

The study was performed in accordance to the guidelines of the Control of Animal Experimentation and Ethical Principles in Animal Research (CONCEA - National Council for Control of Experimental Animals), under the approved protocol n° 702, emitted by the Institute of Bioscience of Botucatu Ethics Committee on Animal Use, from the Sao Paulo State University (UNESP, Brazil).

4.2. Total RNA isolation

RNA extraction was performed using TRIZOL reagent (Thermo Fisher Scientific, USA), according to the manufacturer's instructions. The RNA was quantitated by spectrophotometry (NanoVue; GE Healthcare Life Sciences, USA) and its integrity was ensured by obtaining RNA Integrity Number (RIN) > 8 (Agilent 2100 Bioanalyzer; Agilent Technologies, Germany). RNA samples were treated with DNA Free Kit (Thermo Fisher Scientific, USA) to remove genomic DNA contamination.

4.3. Preparation and processing of mRNA-Seq and miRNA-seq libraries

RNA sequencing libraries were constructed with TruSeq Stranded Total RNA Sample Prep Kits (Illumina, USA) using 1000 ng of total RNA. Samples were indexed with adaptors and submitted for paired-end 2 × 100-bp sequencing using a HiSeq 2000 instrument (Illumina, USA). Sequencing was performed on ten RNA samples in each lane of the flow cell, following the manufacturer's instructions. Each lane produced ~ 600 million raw paired reads. The data output in the fastq file format contained sequence information, including the sequencing quality (Phred quality score). Average Phred scores of ≥20 per position were used for alignment. We used the TruSeq Small RNA Sample Preparation kit (Illumina, San Diego, USA) to prepare the miRNA-Seq libraries, following the manufacturer's instructions. miRNA libraries were 50 bp single-end sequenced by a HiSeq2000 instrument (Illumina, USA). Sequencing was performed on ten RNA samples in one lane of the flow cell.

4.4. Read Alignment and differential gene expression analysis

Paired-end reads for mRNA were mapped to the mm10 genome using TopHat2 [86] with the following options: --mate-inner-dist 200 --mate-std-dev 100 --no-novel-juncs --min-intron-length 40. Single-end reads for miRNA were mapped to the miRBase version 21 using Bowtie [87] with the following options: -n 0 -l 8 -a --best --strata --phred33-quals. Counts for RefSeq genes were obtained using HTSeq [88] with the default settings, and DESeq2 (version 1.4) [89] was used to normalize expression counts. Genes were considered differentially expressed if |fold change| (FC) ≥1.5, and the p-values ≤ 0.05. For assessing mRNA transcript abundance, the reads were converted to reads per thousand base pairs peak per million mapped reads (RPKM). For assessing miRNA abundance, the reads were converted to counts per million mapped reads (CPM).

4.5. Transcriptions factors motif analyses

Pscan web interface [90] (http://159.149.160.88/pscan/) was used to detect DNA motifs overrepresented in each class between nucleotides −300 and +50 relative to the Transcription Start Site (TSS). Significance was tested against CpG-content-matched promoters as background. Binding sites were considered significantly overrepresented when p-value <0.01.

4.6. Gene Ontology (GO) enrichment analysis

GO enrichment was performed with the ClueGO Cytoscape plugin [91], using a hypergeometric test with a Benjamini and Hochberg False Discovery Rate correction [92]. A p-value cut-off of 0.05 was used to identify enriched terms.

4.7. miRNA target prediction

Candidate miRNA-mRNA targets relationships were predicted by at least one or more of the following target prediction algorithms (union set) extracted from mirDB [93], TargetScan 5.1 (conservation and non-conservation sites) [94], DIANA-microT [95], PicTar (4-way, and 5-way) [96]. Additionally, we used validated targets deposited in miRTarBase [97]. We also filtered our data using differentially expressed genes (mRNA and miRNA) identified by RNA-Seq, considering that mRNA and miRNA expression levels should be inversely correlated.

4.7. Interaction network

Based on the differentially expressed genes, protein-protein interaction networks were generated via the STRING database [98,99] (http://string-db.org/), which also detect functional interactions among the corresponding genes. Network visualization was performed using the open-source software platform Cytoscape [100] v. 3.6.1 (https://cytoscape.org/).

4.8. Cell culture

The mouse immortalized myoblast cell line C2C12 (ATCC® CRL-1772™) was used as *in vitro* model. Cells were grown at 37°C, and 5% CO2 in DMEM (Thermo Fisher Scientific, USA) supplemented with 10% fetal bovine serum (Omega Scientific, USA) and 1% Penicillin-Streptomycin (Thermo Fisher Scientific, USA). Myoblasts were induced to differentiate into myotubes by switching the cells to a differentiation medium consisting of DMEM plus 2% horse serum (Thermo Fisher Scientific, USA), for six days. A mixture of TNF-α (10 ng / mL) (Thermo Fisher Scientific, USA) and INF-γ (100 U / mL) (Thermo Fisher Scientific, USA) was added in differentiated myotubes to induce cellular atrophy.

4.9. Immunofluorescence staining

C2C12 myotubes were seeded on a glass slide for five days in differentiation medium. Cells were fixed with 4% paraformaldehyde for 15 minutes. Subsequently, the cells were permeabilized with 0.1% Triton X-100 (Sigma-Aldrich, USA) for 10 minutes on ice. Cells were treated with 8% fetal bovine serum and 3% bovine serum albumin for one hour and then incubated overnight at 4°C with a mouse anti-Skeletal Myosin (M7523, 1:600 dilution, Sigma-Aldrich, USA). After washing in PBS, samples were incubated with a secondary antibody (TRITC, 1:1000 dilution; and Alexa Fluor 488, 1:1000 dilution; Sigma-Aldrich, USA), for 2 hours at room temperature, and subsequently mounted with Vecta Shield-DAPI (Vector Laboratories, USA). Images were collected with a scanning confocal microscope TCS SP5 (Leica Microsystems, UK). The atrophy of myotubes treated with the cytokines was determined by measuring the diameter of at least 50 myotubes for each sample with the ImageJ software (https://imagej.nih.gov/ij/).

4.10. Picrosirius red staining

Cryostat transverse-sections of the TA muscle (10 μm thick) were collected in control and LLC tumor-bearing mice. Collected samples were placed on the same slide to minimize staining differences; sections were incubated with a saturated picric acid solution followed by Picrosirius red (0.1% Sirius red in saturated picric acid) for three minutes, dehydrated and mounted in Permount. Eight color pictures per sample were captured using a light microscope (Olympus, Japan). Light intensity parameters used were the same for all samples. Picrosirius staining areas were assessed using Image J software. As previously described, picrosirius staining areas were normalized for cell

density to account for individual fiber atrophy [101]. To quantify muscle tissue disorganization, we employed fractal dimension analysis by binarizing photographs using the ImageJ software, as previously described [102]. Briefly, the fractal dimension was estimated using box-counting tool (ImageJ software), which quantifies pixels distribution in the space, without considering image texture. The fractal dimension value is expressed from 0 to 2, where values close to 2 represent higher tissue disorganization.

4.11. Western blotting analysis

Muscle proteins were extracted using Tris-Triton buffer (10 mM Tris pH 7.4, 100 mM NaCl, 1 mM EDTA, 1 mM EGTA, 1% Triton X-100, 10% glycerol, 0.1% SDS, 0.5% deoxycholate) containing Protease Inhibitor Cocktail (Sigma-Aldrich, USA) and quantified by the Bradford method [103]. Subsequently, Lammeli buffer (Sigma-Aldrich, USA) was added to each sample and boiled at 100°C for 10 min. Proteins were subjected to SDS-PAGE on 10% polyacrylamide gels. After electrophoresis, proteins were electrotransferred to nitrocellulose membranes (Bio-Rad, USA) for 2 hours at 120V. The membranes were blocked with 5% non-fat dry milk diluted in TBS-Tween for 2 hours, and then incubated overnight at 4°C with collagen I (1:100 dilution, sc-25974, Santa Cruz, USA) or β-actin (1:1000 dilution, sc-81178, Santa Cruz, USA) antibodies. Secondary antibodies conjugated with horseradish peroxidase (HRP) and ECL chemiluminescent detection (GE Healthcare, USA) system was used for visualization of the blots in ImageQuant™ LAS 400 (GE Healthcare, USA). We quantified the blots by densitometry using ImageJ software, and collagen I values were normalized by β-actin.

4.12. Statistical analysis

Data were expressed as mean ± standard deviation (SD). Statistical analysis was performed using the GraphPad Prism software v 6.07 (GraphPad Software, Inc., USA). For all statistical analyses not described elsewhere, Student's t-test was applied to compare the groups. Statistical significance was considered achieved when the p-value was <0.05.

5. Conclusions

In conclusion, our integrative analysis of miRNA-mRNA co-profiles comprehensively characterized regulatory relationships of molecular pathways, including miRNAs targeting ECM-associated genes, which may play a role in the development of muscle atrophy in cancer cachexia. The *in-silico* analyses of the transcriptome data revealed that these ECM genes are potentially regulated post-transcriptionally by miRNAs such as miR-29a-3p. We also confirmed that the cytokines TNF-α and IFN-γ induce transcriptional changes in ECM-associated genes in C2C12 myotubes.

Supplementary Materials: The following are available online at www.mdpi.com/xxx/s1, Figure S1: Lewis Lung Cancer (LLC) cells induce anatomical changes in mice.; Figure S2: Transcriptome characterization of cancer cachexia; Table S1: mRNA differentially expressed in LLC tumor-bearing mice; Table S2: Gene enrichment analysis of differentially expressed genes in LLC tumor-bearing mice; Table S3: Differentially expressed miRNAs in LLC tumor-bearing mice.

Author Contributions: Conceptualization, G.J.F and R.F.C; methodology, G.J.F., J.H.F., I.J.V., L.N.M., S.S.C., P.P.F and J.G ; formal analysis, G.J.F; investigation, G.J.F., and R.F.C.; resources, M.D.P.S., R.F., and R.F.C; data curation, G.J.F., S.R.R., and R.F.C; writing—original draft preparation, G.J.F., and R.F.C; writing—review and editing, all authors; supervision R.F.C.; project administration, R.F.C; funding acquisition, G.J.F., and R.F.C.

Funding: This study was supported by the São Paulo Research Foundation (FAPESP, grants # 12/13961-6 and 13/50343-1, R.F.C). G.J.F received FAPESP fellowships (grants # 16/08294-1, 14/13941-0, 13/02005-0, and 11/16282-0).

Conflicts of Interest: The authors declare no conflict of interest.

References

1. Dhanapal, R.; Saraswathi, T.; Govind, R.N. Cancer cachexia. J. Oral Maxillofac. Pathol. 2011, 15, 257–60.

2. Loberg, R.D.; Bradley, D.A.; Tomlins, S.A.; Chinnaiyan, A.M.; Pienta, K.J. The lethal phenotype of cancer: the molecular basis of death due to malignancy. CA. Cancer J. Clin. 2007, 57, 225–41.

3. Vaughan, V.C.; Martin, P.; Lewandowski, P.A. Cancer cachexia: Impact, mechanisms and emerging treatments. J. Cachexia. Sarcopenia Muscle 2013, 4, 95–109.

4. von Haehling, S.; Anker, M.S.; Anker, S.D. Prevalence and clinical impact of cachexia in chronic illness in Europe, USA, and Japan: facts and numbers update 2016. J. Cachexia. Sarcopenia Muscle 2016, 7, 507–509.

5. Dewys, W.D.; Begg, C.; Lavin, P.T.; Band, P.R.; Bennett, J.M.; Bertino, J.R.; Cohen, M.H.; Douglass, H.O.; Engstrom, P.F.; Ezdinli, E.Z.; et al. Prognostic effect of weight loss prior to chemotherapy in cancer patients. Eastern Cooperative Oncology Group. Am. J. Med. 1980, 69, 491–7.

6. Martin, L.; Birdsell, L.; MacDonald, N.; Reiman, T.; Clandinin, M.T.; McCargar, L.J.; Murphy, R.; Ghosh, S.; Sawyer, M.B.; Baracos, V.E. Cancer cachexia in the age of obesity: Skeletal muscle depletion is a powerful prognostic factor, independent of body mass index. J. Clin. Oncol. 2013, 31, 1539–1547.

7. Fearon, K.C.; Arends, J.; Baracos, V. Understanding the mechanisms and treatment options in cancer cachexia. Nat. Rev. Clin. Oncol. 2013, 10, 90–99.

8. Porporato, P.E. Understanding cachexia as a cancer metabolism syndrome. Oncogenesis 2016, 5, e200.

9. Fearon, K.C.H.; Glass, D.J.; Guttridge, D.C. Cancer cachexia: mediators, signaling, and metabolic pathways. Cell Metab. 2012, 16, 153–66.

10. Monitto, C.L.; Berkowitz, D.; Lee, K.M.; Pin, S.; Li, D.; Breslow, M.; O'Malley, B.; Schiller, M. Differential gene expression in a murine model of cancer cachexia. Am. J. Physiol. Endocrinol. Metab. 2001, 281, E289-97.

11. Blackwell, T.A.; Cervenka, I.; Khatri, B.; Brown, J.L.; Rosa-Caldwell, M.E.; Lee, D.E.; Perry, R.A.; Brown, L.A.; Haynie, W.S.; Wiggs, M.P.; et al. A Transcriptomic Analysis of the Development of Skeletal Muscle Atrophy in Cancer-Cachexia in Tumor-Bearing Mice. Physiol. Genomics. 2018, 50, 1071-1082.

12. Shum, A.M.Y.; Fung, D.C.Y.; Corley, S.M.; McGill, M.C.; Bentley, N.L.; Tan, T.C.; Wilkins, M.R.; Polly, P. Cardiac and skeletal muscles show molecularly distinct responses to cancer cachexia. Physiol. Genomics 2015, 47, 588–99.

13. Bonetto, A.; Aydogdu, T.; Kunzevitzky, N.; Guttridge, D.C.; Khuri, S.; Koniaris, L.G.; Zimmers, T. a STAT3 activation in skeletal muscle links muscle wasting and the acute phase response in cancer cachexia. PLoS One. 2011, 6, e22538.

14. Gallagher, I.J.; Stephens, N. a; MacDonald, A.J.; Skipworth, R.J.E.; Husi, H.; Greig, C. a; Ross, J. a; Timmons, J. a; Fearon, K.C.H. Suppression of skeletal muscle turnover in cancer cachexia: evidence from the transcriptome in sequential human muscle biopsies. Clin. Cancer Res. 2012, 18, 2817–27.

15. Stephens, N. a; Gallagher, I.J.; Rooyackers, O.; Skipworth, R.J.; Tan, B.H.; Marstrand, T.; Ross, J. a; Guttridge, D.C.; Lundell, L.; Fearon, K.C.; et al. Using transcriptomics to identify and validate novel biomarkers of human skeletal muscle cancer cachexia. Genome Med. 2010, 2, 1.

16. Fukawa, T.; Yan-Jiang, B.C.; Min-Wen, J.C.; Jun-Hao, E.T.; Huang, D.; Qian, C.-N.; Ong, P.; Li, Z.; Chen, S.; Mak, S.Y.; et al. Excessive fatty acid oxidation induces muscle atrophy in cancer cachexia. Nat. Med. 2016, 22, 666–671.

17. Fontes-Oliveira, C.C.; Busquets, S.; Fuster, G.; Ametller, E.; Figueras, M.; Olivan, M.; Toledo, M.; López-Soriano, F.J.; Qu, X.; Demuth, J.; et al. A differential pattern of gene expression in skeletal muscle of tumor-

bearing rats reveals dysregulation of excitation–contraction coupling together with additional muscle alterations. Muscle Nerve 2014, 49, 233–48.

18. Judge, S.M.; Wu, C.-L.; Beharry, A.W.; Roberts, B.M.; Ferreira, L.F.; Kandarian, S.C.; Judge, A.R. Genome-wide identification of FoxO-dependent gene networks in skeletal muscle during C26 cancer cachexia. BMC Cancer 2014, 14, 997.

19. Shen, H.; Liu, T.; Fu, L.; Zhao, S.; Fan, B.; Cao, J.; Li, X. Identification of microRNAs involved in dexamethasone-induced muscle atrophy. Mol. Cell. Biochem. 2013, 381, 105–13.

20. Agarwal, P.; Srivastava, R.; Srivastava, A.K.; Ali, S.; Datta, M. MiR-135a targets IRS2 and regulates insulin signaling and glucose uptake in the diabetic gastrocnemius skeletal muscle. Biochim. Biophys. Acta - Mol. Basis Dis. 2013, 1832, 1294–1303.

21. Soares, R.J.; Cagnin, S.; Chemello, F.; Silvestrin, M.; Musaro, A.; De Pitta, C.; Lanfranchi, G.; Sandri, M. Involvement of microRNAs in the regulation of muscle wasting during catabolic conditions. J. Biol. Chem. 2014, 289, 21909–25.

22. Eisenberg, I.; Eran, A.; Nishino, I.; Moggio, M.; Lamperti, C.; Amato, A. a; Lidov, H.G.; Kang, P.B.; North, K.N.; Mitrani-Rosenbaum, S.; et al. Distinctive patterns of microRNA expression in primary muscular disorders. Proc. Natl. Acad. Sci. U. S. A. 2007, 104, 17016–21.

23. Moraes, L.N.; Fernandez, G.J.; Vechetti-Júnior, I.J.; Freire, P.P.; Souza, R.W.A.; Villacis, R.A.R.; Rogatto, S.R.; Reis, P.P.; Dal-Pai-Silva, M.; Carvalho, R.F. Integration of miRNA and mRNA expression profiles reveals microRNA-regulated networks during muscle wasting in cardiac cachexia. Sci. Rep. 2017, 7.

24. Li, J.; Chan, M.C.; Yu, Y.; Bei, Y.; Chen, P.; Zhou, Q.; Cheng, L.; Chen, L.; Ziegler, O.; Rowe, G.C.; et al. miR-29b contributes to multiple types of muscle atrophy. Nat. Commun. 2017, 8, 15201.

25. Narasimhan, A.; Ghosh, S.; Stretch, C.; Greiner, R.; Bathe, O.F.; Baracos, V.; Damaraju, S. Small RNAome profiling from human skeletal muscle: novel miRNAs and their targets associated with cancer cachexia. J. Cachexia. Sarcopenia Muscle. 2017, 8, 405-416.

26. Lee, D.E.; Brown, J.L.; Rosa-Caldwell, M.E.; Blackwell, T.A.; Perry, R.A.; Brown, L.A.; Khatri, B.; Seo, D.; Bottje, W.G.; Washington, T.A.; et al. Cancer Cachexia-Induced Muscle Atrophy: Evidence for Alterations in microRNAs important for Muscle Size. Physiol. Genomics. 2017, 49, 253-260.

27. Dragomir, M.P.; Knutsen, E.; Calin, G.A. SnapShot: Unconventional miRNA Functions. Cell. 2018, 174, 1038-1038.e1.

28. Flynt, A.S.; Lai, E.C. Biological principles of microRNA-mediated regulation: shared themes amid diversity. Nat. Rev. Genet. 2008, 9, 831–842.

29. Hulmi, J.J.; Silvennoinen, M.; Lehti, M.; Kivelä, R.; Kainulainen, H. Altered REDD1, myostatin, and Akt/mTOR/FoxO/MAPK signaling in streptozotocin-induced diabetic muscle atrophy. Am. J. Physiol. Endocrinol. Metab. 2012, 302, E307-15.

30. Bodine, S.C.; Stitt, T.N.; Gonzalez, M.; Kline, W.O.; Stover, G.L.; Bauerlein, R.; Zlotchenko, E.; Scrimgeour, A.; Lawrence, J.C.; Glass, D.J.; et al. Akt/mTOR pathway is a crucial regulator of skeletal muscle hypertrophy and can prevent muscle atrophy in vivo. Nat. Cell Biol. 2001, 3, 1014–1019.

31. Nuoc, T.-N.; Kim, S.; Ahn, S.H.; Lee, J.-S.; Park, B.-J.; Lee, T.-H. The analysis of antioxidant expression during muscle atrophy induced by hindlimb suspension in mice. J. Physiol. Sci. 2017, 67, 121–129.

32. Di Foggia, V.; Zhang, X.; Licastro, D.; Gerli, M.F.M.; Phadke, R.; Muntoni, F.; Mourikis, P.; Tajbakhsh, S.; Ellis, M.; Greaves, L.C.; et al. Bmi1 enhances skeletal muscle regeneration through MT1-mediated oxidative stress protection in a mouse model of dystrophinopathy. J. Exp. Med. 2014, 211, 2617–2633.

33. Summermatter, S.; Bouzan, A.; Pierrel, E.; Melly, S.; Stauffer, D.; Gutzwiller, S.; Nolin, E.; Dornelas, C.; Fryer, C.; Leighton-Davies, J.; et al. Blockade of Metallothioneins 1 and 2 Increases Skeletal Muscle Mass and Strength. Mol. Cell. Biol. 2017, 37, 1–11.

34. Sun, Y.; Li, Y.; Wang, H.; Li, H.; Liu, S.; Chen, J.; Ying, H. miR-146a-5p acts as a negative regulator of TGF-β signaling in skeletal muscle after acute contusion. Acta Biochim. Biophys. Sin. (Shanghai). 2017, 49, 628–634.

35. Naguibneva, I.; Ameyar-Zazoua, M.; Polesskaya, A.; Ait-Si-Ali, S.; Groisman, R.; Souidi, M.; Cuvellier, S.; Harel-Bellan, A. The microRNA miR-181 targets the homeobox protein Hox-A11 during mammalian myoblast differentiation. Nat. Cell Biol. 2006, 8, 278–84.

36. Moraes, L.N.; Fernandez, G.J.; Vechetti-Júnior, I.J.; Freire, P.P.; Souza, R.W.A.; Villacis, R.A.R.; Rogatto, S.R.; Reis, P.P.; Dal-Pai-Silva, M.; Carvalho, R.F. Integration of miRNA and mRNA expression profiles reveals microRNA-regulated networks during muscle wasting in cardiac cachexia. Sci. Rep. 2017, 7, 1–13.

37. Langstein, H.N.; Doherty, G.M.; Fraker, D.L.; Buresh, C.M.; Norton, J.A. The roles of gamma-interferon and tumor necrosis factor alpha in an experimental rat model of cancer cachexia. Cancer Res. 1991, 51, 2302–6.

38. Ma, J.F.; Sanchez, B.J.; Hall, D.T.; Tremblay, A.K.; Di Marco, S.; Gallouzi, I. STAT3 promotes IFNγ/TNFα-induced muscle wasting in an NF-κB-dependent and IL-6-independent manner. EMBO Mol. Med. 2017, 9, 622–637.

39. Baracos, V.E.; Martin, L.; Korc, M.; Guttridge, D.C.; Fearon, K.C.H. Cancer-associated cachexia. Nat. Rev. Dis. Prim. 2018, 4, 17105.

40. Matsuyama, T.; Ishikawa, T.; Okayama, T.; Oka, K.; Adachi, S.; Mizushima, K.; Kimura, R.; Okajima, M.; Sakai, H.; Sakamoto, N.; et al. Tumor inoculation site affects the development of cancer cachexia and muscle wasting. Int. J. Cancer 2015, 137, 2558–2565.

41. Norden, D.M.; Devine, R.; McCarthy, D.O.; Wold, L.E. Storage Conditions and Passages Alter IL-6 secretion in C26 adenocarcinoma cell lines. MethodsX 2015, 2, 53–58.

42. Prado, C.M.; Sawyer, M.B.; Ghosh, S.; Lieffers, J.R.; Esfandiari, N.; Antoun, S.; Baracos, V.E. Central tenet of cancer cachexia therapy: do patients with advanced cancer have exploitable anabolic potential? Am. J. Clin. Nutr. 2013, 98, 1012–9.

43. Johns, N.; Stretch, C.; Tan, B.H.L.; Solheim, T.S.; S??rhaug, S.; Stephens, N.A.; Gioulbasanis, I.; Skipworth, R.J.E.; Deans, D.A.C.; Vigano, A.; et al. New genetic signatures associated with cancer cachexia as defined by low skeletal muscle index and weight loss. J. Cachexia. Sarcopenia Muscle. 2017, 8, 122-130.

44. Eldar, A.; Elowitz, M.B. Functional roles for noise in genetic circuits. Nature. 2010, 467, 167–173.

45. Guan, J.; Yang, E.; Yang, J.; Zeng, Y.; Ji, G.; Cai, J.J. Exploiting aberrant mRNA expression in autism for gene discovery and diagnosis. Hum. Genet. 2016, 135, 797–811.

46. Zhang, F.; Shugart, Y.Y.; Yue, W.; Cheng, Z.; Wang, G.; Zhou, Z.; Jin, C.; Yuan, J.; Liu, S.; Xu, Y. Increased Variability of Genomic Transcription in Schizophrenia. Sci. Rep. 2015, 5, 3–6.

47. Ecker, S.; Pancaldi, V.; Rico, D.; Valencia, A. Higher gene expression variability in the more aggressive subtype of chronic lymphocytic leukemia. Genome Med. 2015, 7, 1–12.

48. Mar, J.C.; Matigian, N.A.; Mackay-Sim, A.; Mellick, G.D.; Sue, C.M.; Silburn, P.A.; McGrath, J.J.; Quackenbush, J.; Wells, C.A. Variance of gene expression identifies altered network constraints in neurological disease. PLoS Genet. 2011, 7.

49. Gerstein, M.B.; Kundaje, A.; Hariharan, M.; Landt, S.G.; Yan, K.-K.; Cheng, C.; Mu, X.J.; Khurana, E.; Rozowsky, J.; Alexander, R.; et al. Architecture of the human regulatory network derived from ENCODE data. Nature 2012, 489, 91–100.

50. Cai, D.; Frantz, J.D.; Tawa, N.E.; Melendez, P.A.; Oh, B.; Lidov, H.G.W.; Hasselgren, P.; Frontera, W.R.; Lee, J.; Glass, D.J.; et al. IKKbeta/NF-kappaB activation causes severe muscle wasting in mice. Cell 2004, 119, 285–98.

51. Choi, M.-C.; Cohen, T.J.; Barrientos, T.; Wang, B.; Li, M.; Simmons, B.J.; Yang, J.S.; Cox, G.A.; Zhao, Y.; Yao, T.-P. A direct HDAC4-MAP kinase crosstalk activates muscle atrophy program. Mol. Cell 2012, 47, 122–32.

52. Costelli, P.; Muscaritoli, M.; Bossola, M.; Crepaldi, S.; Sperimentale, O.; Torino, U.; Clinica, M.; Sapienza, U. La; Chirurgica, C.; Cattolica, U. Skeletal muscle wasting in tumor-bearing rats is associated with MyoD down-regulation. Int J Oncol. 2005, 1663–1668.

53. Zhang, L.; Pan, J.; Dong, Y.; Tweardy, D.J.; Dong, Y.; Garibotto, G.; Mitch, W.E. Stat3 activation links a C/EBPδ to myostatin pathway to stimulate loss of muscle mass. Cell Metab. 2013, 18, 368–379.

54. Chen, J.L.; Walton, K.L.; Hagg, A.; Colgan, T.D.; Johnson, K.; Qian, H.; Gregorevic, P.; Harrison, C.A. Specific targeting of TGF-β family ligands demonstrates distinct roles in the regulation of muscle mass in health and disease. Proc. Natl. Acad. Sci. 2017, E5266-E5275.

55. Berkes, C.A.; Bergstrom, D.A.; Penn, B.H.; Seaver, K.J.; Knoepfler, P.S.; Tapscott, S.J. Pbx marks genes for activation by MyoD indicating a role for a homeodomain protein in establishing myogenic potential. Mol. Cell 2004, 14, 465–477.

56. Watanabe, S.; Kondo, S.; Hayasaka, M.; Hanaoka, K. Functional analysis of homeodomain-containing transcription factor Lbx1 in satellite cells of mouse skeletal muscle. J. Cell Sci. 2007, 120, 4178–87.

57. Rossi, G.; Antonini, S.; Bonfanti, C.; Monteverde, S.; Vezzali, C.; Tajbakhsh, S.; Cossu, G.; Messina, G. Nfix Regulates Temporal Progression of Muscle Regeneration through Modulation of Myostatin Expression. Cell Rep. 2016, 14, 2238–2249.

58. Chen, W.; Zhang, X.; Birsoy, K.; Roeder, R.G. A muscle-specific knockout implicates nuclear receptor coactivator MED1 in the regulation of glucose and energy metabolism. Proc. Natl. Acad. Sci. U. S. A. 2010, 107, 10196–201.

59. Tsika, R.W.; Schramm, C.; Simmer, G.; Fitzsimons, D.P.; Moss, R.L.; Ji, J. Overexpression of TEAD-1 in transgenic mouse striated muscles produces a slower skeletal muscle contractile phenotype. J. Biol. Chem. 2008, 283, 36154–36167.

60. Grifone, R.; Laclef, C.; Spitz, F.; Lopez, S.; Demignon, J.; Guidotti, J.-E.; Kawakami, K.; Xu, P.-X.; Kelly, R.; Petrof, B.J.; et al. Six1 and Eya1 expression can reprogram adult muscle from the slow-twitch phenotype into the fast-twitch phenotype. Mol. Cell. Biol. 2004, 24, 6253–6267.

61. Pacini, L.; Suffredini, S.; Ponti, D.; Coppini, R.; Frati, G.; Ragona, G.; Cerbai, E.; Calogero, A. Altered calcium regulation in isolated cardiomyocytes from Egr-1 knock-out mice. Can. J. Physiol. Pharmacol. 2013, 91, 1135–1142.

62. Asp, P.; Acosta-Alvear, D.; Tsikitis, M.; van Oevelen, C.; Dynlacht, B.D. E2f3b plays an essential role in myogenic differentiation through isoform-specific gene regulation. Genes Dev. 2009, 23, 37–53.

63. Zhou, L.; Sun, K.; Zhao, Y.; Zhang, S.; Wang, X.; Li, Y.; Lu, L.; Chen, X.; Chen, F.; Bao, X.; et al. Linc-YY1 promotes myogenic differentiation and muscle regeneration through an interaction with the transcription factor YY1. Nat. Commun. 2015, 6.

64. An, H.T.; Kim, J.; Yoo, S.; Ko, J. Small leucine zipper protein (sLZIP) negatively regulates skeletal muscle differentiation via interaction with ??-actinin-4. J. Biol. Chem. 2014, 289, 4969–4979.

65. Jheng, J.R.; Chen, Y.S.; Ao, U.I.; Chan, D.C.; Huang, J.W.; Hung, K.Y.; Tarng, D.C.; Chiang, C.K. The double-edged sword of endoplasmic reticulum stress in uremic sarcopenia through myogenesis perturbation. J. Cachexia. Sarcopenia Muscle 2018, 9, 570–584.

66. LaBarge, S.; McDonald, M.; Smith-Powell, L.; Auwerx, J.; Huss, J.M. Estrogen-related receptor-α (ERRα) deficiency in skeletal muscle impairs regeneration in response to injury. FASEB J. 2014, 28, 1082–1097.

67. Moretti, I.; Ciciliot, S.; Dyar, K.A.; Abraham, R.; Murgia, M.; Agatea, L.; Akimoto, T.; Bicciato, S.; Forcato, M.; Pierre, P.; et al. MRF4 negatively regulates adult skeletal muscle growth by repressing MEF2 activity. Nat. Commun. 2016, 7, 1–12.

68. Moresi, V.; Williams, A.H.; Meadows, E.; Flynn, J.M.; Potthoff, M.J.; McAnally, J.; Shelton, J.M.; Backs, J.; Klein, W.H.; Richardson, J.A.; et al. Myogenin and class II HDACs control neurogenic muscle atrophy by inducing E3 ubiquitin ligases. Cell 2010, 143, 35–45.

69. Reiter, F.; Wienerroither, S.; Stark, A. Combinatorial function of transcription factors and cofactors. Curr. Opin. Genet. Dev. 2017, 43, 73–81.

70. Cheng, C.S.; Behar, M.S.; Suryawanshi, G.W.; Feldman, K.E.; Spreafico, R.; Hoffmann, A. Iterative Modeling Reveals Evidence of Sequential Transcriptional Control Mechanisms. Cell Syst. 2017, 4, 330-343.e5.

71. Bartel, D.P. Metazoan MicroRNAs. Cell 2018, 173, 20–51.

72. Wang, H.; Garzon, R.; Sun, H.; Ladner, K.J.; Singh, R.; Dahlman, J.; Cheng, A.; Hall, B.M.; Qualman, S.J.; Chandler, D.S.; et al. NF-kappaB-YY1-miR-29 regulatory circuitry in skeletal myogenesis and rhabdomyosarcoma. Cancer Cell 2008, 14, 369–81.

73. Zhou, L.; Wang, L.; Lu, L.; Jiang, P.; Sun, H.; Wang, H. Inhibition of miR-29 by TGF-beta-Smad3 signaling through dual mechanisms promotes transdifferentiation of mouse myoblasts into myofibroblasts. PLoS One 2012, 7, e33766.

74. Zhou, L.; Wang, L.; Lu, L.; Jiang, P.; Sun, H.; Wang, H. A Novel Target of MicroRNA-29, Ring1 and YY1-binding Protein (Rybp), Negatively Regulates Skeletal Myogenesis. J. Biol. Chem. 2012, 287, 25255–65.

75. Park, S.Y.; Lee, J.H.; Ha, M.; Nam, J.W.; Kim, V.N. miR-29 miRNAs activate p53 by targeting p85α and CDC42. Nat. Struct. Mol. Biol. 2009, 16, 23–29.

76. Gao, S.; Cheng, C.; Chen, H.; Li, M.; Liu, K.; Wang, G. IGF1 3′UTR functions as a ceRNA in promoting angiogenesis by sponging miR-29 family in osteosarcoma. J. Mol. Histol. 2016, 47, 135–143.

77. Soares, R.J.; Cagnin, S.; Chemello, F.; Silvestrin, M.; Musaro, A.; De Pitta, C.; Lanfranchi, G.; Sandri, M. Involvement of microRNAs in the regulation of muscle wasting during catabolic conditions. J. Biol. Chem. 2014, 289, 21909–25.

78. Ebert, M.S.; Sharp, P. a Roles for microRNAs in conferring robustness to biological processes. Cell 2012, 149, 515–24.

79. Carroll, A.P.; Goodall, G.J.; Liu, B. Understanding principles of miRNA target recognition and function through integrated biological and bioinformatics approaches. Wiley Interdiscip. Rev. RNA 2014, 5, 361–379.

80. He, W.A.; Berardi, E.; Cardillo, V.M.; Acharyya, S.; Aulino, P.; Thomas-Ahner, J.; Wang, J.; Bloomston, M.; Muscarella, P.; Nau, P.; et al. NF-κB-mediated Pax7 dysregulation in the muscle microenvironment promotes cancer cachexia. J. Clin. Invest. 2013, 1–15.

81. Grande, J.P.; Melder, D.C.; Zinsmeister, A.R. Modulation of collagen gene expression by cytokines: stimulatory effect of transforming growth factor-beta1, with divergent effects of epidermal growth factor and tumor necrosis factor-alpha on collagen type I and collagen type IV. J. Lab. Clin. Med. 1997, 130, 476–86.

82. Verrecchia, F.; Mauviel, A. TGF-beta and TNF-alpha: antagonistic cytokines controlling type I collagen gene expression. Cell. Signal. 2004, 16, 873–80.

83. Kouba, D.J.; Chung, K.; Nishiyama, T.; Vindevoghel, L.; Kon, A.; Klement, J.F.; Mauviel, A. Nuclear Factor-κ B Mediates TNF- α Inhibitory Effect on α 2(I) Collagen (COL1A2) Gene Transcription in Human Dermal Fibroblasts. 2015, 2.

84. Xu, Y.; Harton, J.A.; Smith, B.D. CIITA mediates interferon-γ repression of collagen transcription through phosphorylation-dependent interactions with co-repressor molecules. J. Biol. Chem. 2008, 283, 1243–1256.

85. Freire, P.P.; Cury, S.S.; de Oliveira, G.; Fernandez, G.J.; Moraes, L.N.; da Silva Duran, B.O.; Ferreira, J.H.; Fuziwara, C.S.; Kimura, E.T.; Dal-Pai-Silva, M.; et al. Osteoglycin inhibition by microRNA miR-155 impairs myogenesis. PLoS One 2017, 12, e0188464.

86. Kim, D.; Pertea, G.; Trapnell, C.; Pimentel, H.; Kelley, R.; Salzberg, S.L. TopHat2: accurate alignment of transcriptomes in the presence of insertions, deletions and gene fusions. Genome Biol. 2013, 14, R36.

87. Langmead, B.; Trapnell, C.; Pop, M.; Salzberg, S. Ultrafast and memory-efficient alignment of short DNA sequences to the human genome. Genome Biol. 2009, 10, R25.

88. Anders, S.; Pyl, P.T.; Huber, W. HTSeq-A Python framework to work with high-throughput sequencing data. Bioinformatics 2015, 31, 166–169.

89. Love, M.I.; Huber, W.; Anders, S. Moderated estimation of fold change and dispersion for RNA-seq data with DESeq2. Genome Biol. 2014, 15, 550.

90. Zambelli, F.; Pesole, G.; Pavesi, G. Pscan: finding over-represented transcription factor binding site motifs in sequences from co-regulated or co-expressed genes. Nucleic Acids Res. 2009, 37, W247–W252.

91. Bindea, G.; Mlecnik, B.; Hackl, H.; Charoentong, P.; Tosolini, M.; Kirilovsky, A.; Fridman, W.-H.; Pagès, F.; Trajanoski, Z.; Galon, J. ClueGO: a Cytoscape plug-in to decipher functionally grouped gene ontology and pathway annotation networks. Bioinformatics 2009, 25, 1091–3.

92. Benjamini, Y.; Hochberg, Y. Controlling the False Discovery Rate: A Practical and Powerful Approach to Multiple Testing. J. R. Stat. Soc. Ser. B 1995, 57, 289–300.

93. Wang, X. miRDB: a microRNA target prediction and functional annotation database with a wiki interface. RNA 2008, 14, 1012–7.

94. Garcia, D.M.; Baek, D.; Shin, C.; Bell, G.W.; Grimson, A.; Bartel, D.P. Weak seed-pairing stability and high target-site abundance decrease the proficiency of lsy-6 and other microRNAs. Nat. Struct. Mol. Biol. 2011, 18, 1139–46.

95. Maragkakis, M.; Reczko, M.; Simossis, V. a; Alexiou, P.; Papadopoulos, G.L.; Dalamagas, T.; Giannopoulos, G.; Goumas, G.; Koukis, E.; Kourtis, K.; et al. DIANA-microT web server: elucidating microRNA functions through target prediction. Nucleic Acids Res. 2009, 37, W273-6.

96. Krek, A.; Grün, D.; Poy, M.N.; Wolf, R.; Rosenberg, L.; Epstein, E.J.; MacMenamin, P.; da Piedade, I.; Gunsalus, K.C.; Stoffel, M.; et al. Combinatorial microRNA target predictions. Nat. Genet. 2005, 37, 495–500.

97. Hsu, S.-D.; Lin, F.-M.; Wu, W.-Y.; Liang, C.; Huang, W.-C.; Chan, W.-L.; Tsai, W.-T.; Chen, G.-Z.; Lee, C.-J.; Chiu, C.-M.; et al. miRTarBase: a database curates experimentally validated microRNA-target interactions. Nucleic Acids Res. 2011, 39, D163-9.

98. Snel, B.; Lehmann, G.; Bork, P.; Huynen, M.A. STRING: a web-server to retrieve and display the repeatedly occurring neighbourhood of a gene. Nucleic Acids Res. 2000, 28, 3442–4.

99. Szklarczyk, D.; Morris, J.H.; Cook, H.; Kuhn, M.; Wyder, S.; Simonovic, M.; Santos, A.; Doncheva, N.T.; Roth, A.; Bork, P.; et al. The STRING database in 2017: quality-controlled protein–protein association networks, made broadly accessible. Nucleic Acids Res. 2017, 45, D362–D368.

100. Shannon, P.; Markiel, A.; Ozier, O.; Baliga, N.S.; Wang, J.T.; Ramage, D.; Amin, N.; Schwikowski, B.; Ideker, T. Cytoscape: a software environment for integrated models of biomolecular interaction networks. Genome Res. 2003, 13, 2498–504.

101. Kirby, L.S.; Kirby, M.A.; Warren, J.W.; Tran, L.T.; Yellon, S.M. Increased innervation and ripening of the prepartum murine cervix. J. Soc. Gynecol. Investig. 2005, 12, 578–85.

102. Pacagnelli, F.L.; Sabela, A.K.D. de A.; Mariano, T.B.; Ozaki, G.A.T.; Castoldi, R.C.; Carmo, E.M. do; Carvalho, R.F.; Tomasi, L.C.; Okoshi, K.; Vanderlei, L.C.M. Fractal Dimension in Quantifying Experimental-Pulmonary-Hypertension-Induced Cardiac Dysfunction in Rats. Arq. Bras. Cardiol. 2016, 107, 33-9.

103. Bradford, M.M. A rapid and sensitive method for the quantitation of microgram quantities of protein utilizing the principle of protein-dye binding. Anal. Biochem. 1976, 72, 248–54.